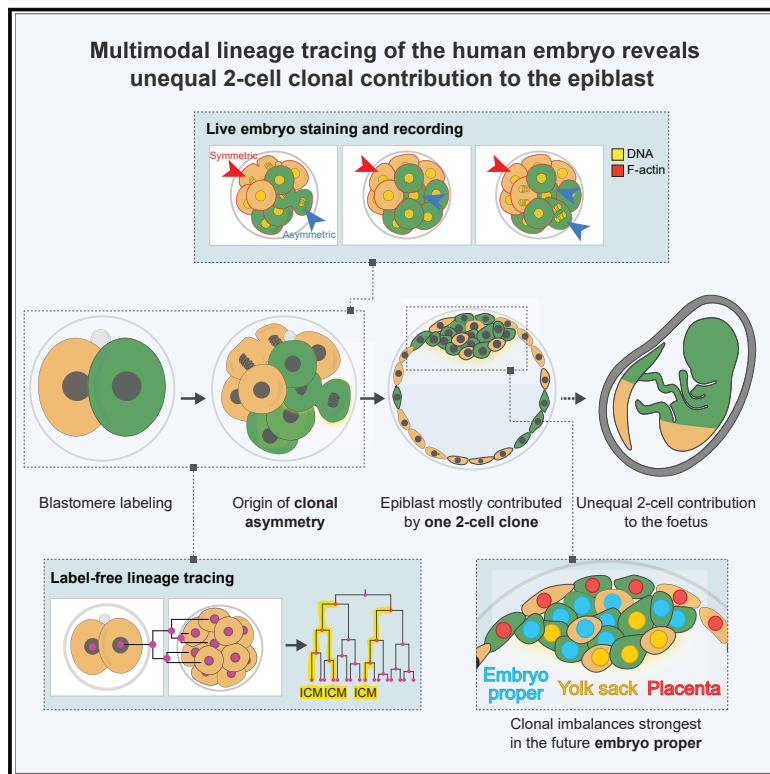


The first two blastomeres contribute unequally to the human embryo

Graphical abstract



Authors

Sergi Junyent, Maciej Meglicki,
Roman Vetter, ..., Richard J. Paulson,
Dagmar Iber, Magdalena Zernicka-Goetz

Correspondence

magdaz@caltech.edu

In brief

Labeling and live imaging of human embryos reveal that the majority of the future body originates, mostly, from one of the 2-cell stage blastomeres. Descendants of the first 2-cell stage blastomere to divide contribute more asymmetric divisions at the 8-cell stage, which generate the small number of founding epiblast cells before implantation.

Highlights

- Lineage tracing of human embryos from the 2-cell to the blastocyst stage
- The majority of the epiblast is derived from only one 2-cell stage blastomere
- Early asymmetric divisions are a bottleneck controlling the embryo's clonal composition
- First-dividing 2-cell blastomere generates more asymmetric divisions at 8-cell stage



Article

The first two blastomeres contribute unequally to the human embryo

Sergi Junyent,^{1,7} Maciej Meglicki,^{2,7} Roman Vetter,^{4,5} Rachel Mandelbaum,³ Catherine King,² Ekta M. Patel,¹ Lisa Iwamoto-Stohl,² Clare Reynell,¹ Dong-Yuan Chen,¹ Patrizia Rubino,³ Nabil Arrach,⁶ Richard J. Paulson,³ Dagmar Iber,^{4,5} and Magdalena Zernicka-Goetz^{1,2,8,*}

¹Division of Biology and Biological Engineering, California Institute of Technology, Pasadena, CA 91125, USA

²Department of Physiology, Development and Neuroscience, University of Cambridge, Cambridge CB2 3EG, UK

³Division of Reproductive Endocrinology and Infertility, Department of Obstetrics and Gynecology, University of Southern California, Los Angeles, CA 90033, USA

⁴Department of Biosystems Science and Engineering (D-BSSE), ETH Zürich, Basel 4058, Switzerland

⁵Swiss Institute of Bioinformatics (SIB), Mattenstrasse 26, 4058 Basel, Switzerland

⁶Progenesis Inc, La Jolla, CA 92037, USA

⁷These authors contributed equally

⁸Lead contact

*Correspondence: magdaz@caltech.edu

<https://doi.org/10.1016/j.cell.2024.04.029>

SUMMARY

Retrospective lineage reconstruction of humans predicts that dramatic clonal imbalances in the body can be traced to the 2-cell stage embryo. However, whether and how such clonal asymmetries arise in the embryo is unclear. Here, we performed prospective lineage tracing of human embryos using live imaging, non-invasive cell labeling, and computational predictions to determine the contribution of each 2-cell stage blastomere to the epiblast (body), hypoblast (yolk sac), and trophectoderm (placenta). We show that the majority of epiblast cells originate from only one blastomere of the 2-cell stage embryo. We observe that only one to three cells become internalized at the 8-to-16-cell stage transition. Moreover, these internalized cells are more frequently derived from the first cell to divide at the 2-cell stage. We propose that cell division dynamics and a cell internalization bottleneck in the early embryo establish asymmetry in the clonal composition of the future human body.

INTRODUCTION

After fertilization, the zygote divides to generate cells that are thought to remain equivalent to each other until the first fate diversification event. This delayed fate specification would predict that each cell of the 2-cell embryo gives rise to, on average, half of all the cells in our bodies. However, genome sequence and single nucleotide polymorphism-based retrospective lineage reconstruction of human development have suggested clonal imbalances in the human body,^{1–5} such that one cell from the 2-cell embryo is often dominant.^{2–5} The reason behind this imbalance is not known. Indeed, when and how cell fate decisions are initiated in the human embryo remain long-standing questions,^{6,7} because the access to human embryos for research is extremely limited.

During embryo development, the first three fates are specified by three successive waves of asymmetric cell divisions (ACDs) that position one daughter cell inside the embryo (inner cell mass [ICM]) and the other on the outside. Cells positioned to the outside generate trophectoderm (TE, future placenta). Intriguingly, in mouse embryos, cells internalized during the first

wave (8-to-16-cell stage) contribute mainly to epiblast (EPI; future body), whereas those internalized during the second (16-to-32-cell stage) and third waves (32-to-64-cell stage) tend to generate primitive endoderm (hypoblast [HYPO] in human, future yolk sac).⁸ Therefore, the number and timing of internalized cells influences the clonal composition of the future mouse body.^{8–11} Whether successive specification of the inner cells happens in human embryos is not known.

Although both blastomeres of the 2-cell mouse embryo and most blastomeres in 4-cell embryos contribute to both ICM and TE,^{12–14} lineage tracing and single-cell RNA sequencing studies suggest that the fate and developmental potential of mouse blastomeres at the 2-cell and 4-cell stages are unequal.^{15–19} Molecular asymmetries in gene expression and epigenetic modifications at the 2-cell and 4-cell stages were found to contribute to their fate.^{16,17,20–22} Importantly, the primary bias of mouse blastomeres is compatible with developmental plasticity; the two can co-exist.^{23,24}

To determine how early blastomeres contribute to the three lineages of the human embryo, we performed lineage tracing of live human embryos from the first cleavage division until the



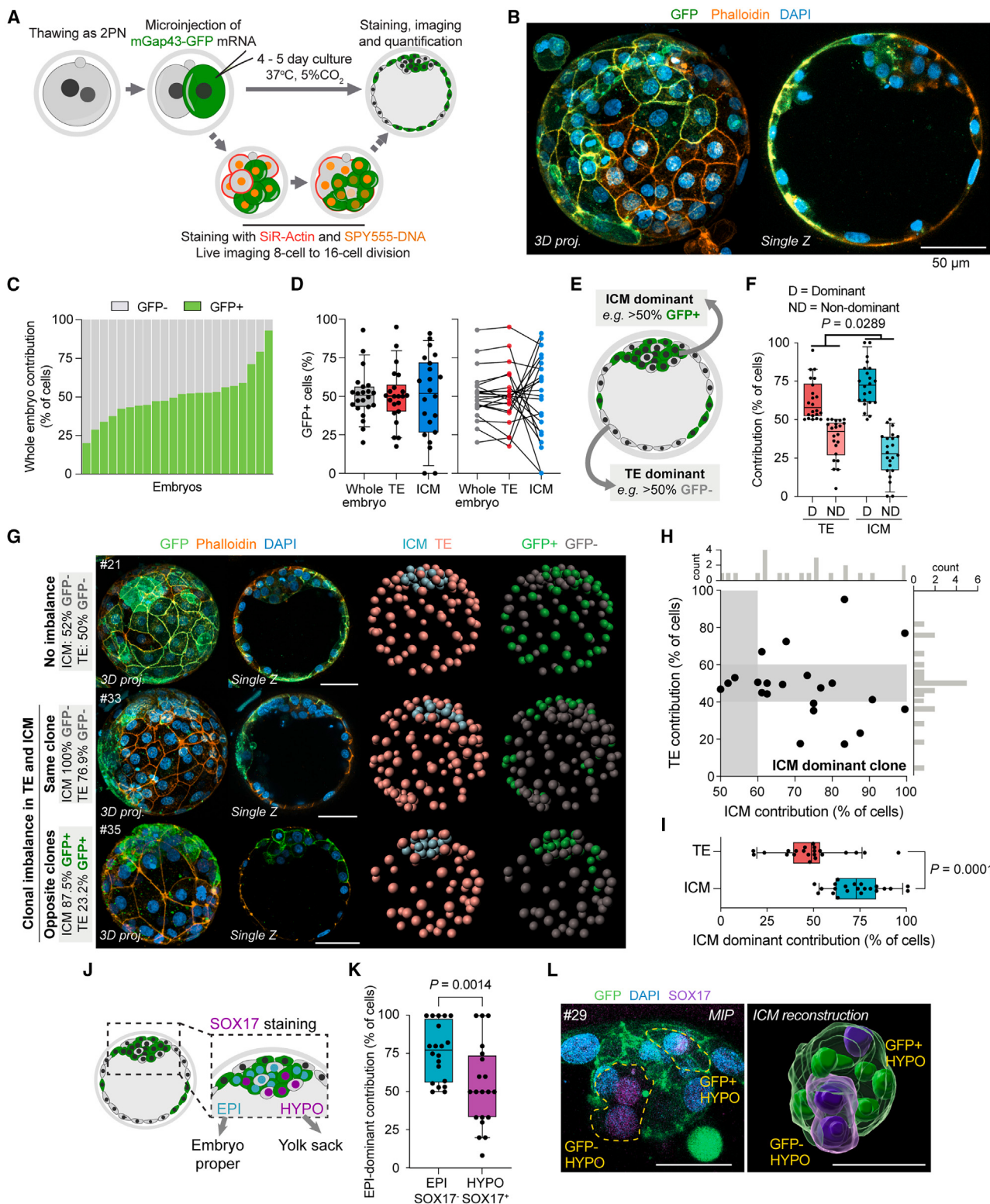


Figure 1. Lineage tracing of 2-cell stage human blastomeres in the blastocyst

(A) Pipeline of the experiment.

(B) Human blastocyst with mosaic GFP expression, stained with AF647-phalloidin and DAPI. Scale bar, 50 μm.

(legend continued on next page)

blastocyst stage. We discovered that the majority of cells in the EPI, the future human body, originate from one of the two cells in most embryos. Notably, the first blastomere to divide at the 2-cell stage has a higher likelihood to generate the first, and more, internalized cells at the 8-to-16-cell stage. We propose that the limited number of cell internalizations at the first wave of ACDs in the human embryo is a bottleneck that creates a large clonal imbalance in the EPI. Our data suggest that an interplay of cell division dynamics and a cell internalization bottleneck in the early embryo leads to clonal asymmetries in the human body.

RESULTS

Lineage tracing of human 2-cell stage blastomeres

Retrospective tracking of somatic mutations in the human body and placenta predicts clonal imbalances may arise as early as the 2-cell stage of the embryo.^{1–5} To determine whether this is indeed the case, we aimed to track forward the lineages of early-stage blastomeres of human embryos. Such prospective studies of human development are challenged by limited availability of human embryos at the zygote stage. Nevertheless, we were able to obtain 54 human *in vitro* fertilized zygotes that had been donated for research.

First, we used a neutral lineage reporter to follow the progeny of individual 2-cell blastomeres through their development to the TE and ICM of the human blastocyst (Figure 1A). Briefly, we thawed human zygotes and cultured them until the completion of the first cleavage division. At the late 2-cell stage (approximately 17 h post-thawing), we microinjected one random blastomere with mRNA encoding GFP fused to the membrane targeting sequence of GAP43 (i.e., not full length, mGap43-GFP; STAR Methods), which has been reported to not affect embryo development. mGap43-GFP marked the boundaries of injected blastomere and its progeny, allowing us to discern lineages from each 2-cell blastomere as GFP-positive (GFP+) versus GFP-negative (GFP−).

We cultured embryos for 4–5 days and fixed them as expanded blastocysts, which we stained with AF647-phalloidin to detect F-actin networks and DAPI to detect chromatin. Blastocysts displayed mosaic GFP expression throughout the TE and

the ICM (Figures 1B and S1B) and had a healthy morphology (Figures S1C–S1E). We found 97.3 ± 27 (mean \pm SD) cells in the whole embryo, 80.8 ± 24 cells in TE, and 16.5 ± 7 cells in ICM, which comprised 11.8 ± 5 EPI cells and 5.2 ± 3 HYPO cells (Figures S1F–S1H), as expected.^{25–29} The number of HYPO cells positively correlated with the overall ICM cell number (Figure S1I), as expected. Each of the 22 analyzed blastocysts contained GFP+ and GFP− cells that contributed to both TE and ICM (Figures 1C, 1D, and S1J). These results show that our lineage tracing does not affect human development or the developmental capacity of the injected blastomere.

2-cell stage human blastomeres contribute unequally to ICM, EPI, and polar TE

To determine the contribution of each 2-cell stage blastomere to all three embryo lineages, we quantified the percentage of GFP+ and GFP− cells in each lineage. The mean frequency of GFP+ cells in the population was ~50% in the whole embryo (50.8% or 48.8 ± 19 cells) as well as the TE and ICM (50.3% or 36.3 ± 22 cells in TE and 49.4% or 7.4 ± 6 cells in the ICM) (Figures 1C and 1D). The differential GFP labeling allowed us to discern the dominant (contributing >50% of cells) and non-dominant populations in the ICM and TE of each blastocyst (Figure 1E). In the ICM, the dominant population accounted for, on average, 71.25% of cells (11.7 ± 5 cells). By contrast, the TE-dominant population accounted for, on average, 62.86% of cells in the TE (51 ± 19 cells) (Figure 1F). The dominant population in either compartment was GFP+ or GFP− with a near-equal chance (Figure S1K), confirming that GFP expression did not affect blastomere development.

We then explored the contribution of each 2-cell clone to the ICM and TE in each individual embryo (Figures 1G–1I). Both 2-cell blastomeres contributed near-equal amounts of cells to the ICM in only 3/22 blastocysts (13.7%), whereas a single 2-cell clone contributed between 60% and 100% of ICM cells in 19/22 embryos (86.3%), pointing to a clonal imbalance in their ICM (Figures 1G and 1H). 10/22 embryos (45%) displayed a clonally imbalanced TE, with 4/22 embryos having ≥60% ICM and TE cells originating from the same 2-cell blastomere (Figures 1G, 1H, and S1L). On average, the ICM-dominant clone, which

(C) Frequency of GFP+ and GFP− cells for each embryo quantified.

(D) (Left) Percentage of GFP+ cells in the whole embryo, TE, or ICM. (Right) Contribution of GFP+ cells in the whole embryo, TE or ICM for each embryo, connected.

(E) Terminology used. The population (GFP+ or GFP−) that contributed >50% to each compartment (ICM or TE) was considered dominant for that compartment. The ICM-dominant population was used as reference, and the matching population in the TE was called “ICM-dominant population in the TE.”

(F) Contribution of dominant (D) or non-dominant (ND) cells to TE and ICM. Statistically significant difference (ICM versus TE) of differences (dominant versus non-dominant, t test).

(G) Human blastocysts with different clonal imbalances in ICM and TE. Spots label the cell centers, colored for TE, ICM, GFP+, or GFP−. Contribution of ICM-dominant cells to each compartment is displayed. Scale bars, 50 μm.

(H) Contribution of ICM-dominant cells to ICM and TE. Marginal histograms indicate distribution. Gray areas represent contribution 50%–60% to ICM and 40%–60% to TE.

(I) Contribution of ICM-dominant cells to TE or ICM. Statistical significance: t test.

(J) SOX17 staining differentiating epiblast (EPI) and hypoblast (HYPO) in ICM.

(K) Contribution of EPI-dominant population to EPI or HYPO. Statistical significance: t test. Two blastocysts from the pilot experiment were not included in the analysis (see STAR Methods, n = 20 blastocysts).

(L) Maximum intensity projection (MIP, left) or reconstruction (right) of a mostly GFP+ ICM containing GFP+ and GFP− hypoblast cells. Scale bars, 25 μm.

For (C), (D), (G), and (I), n = 22 blastocysts. For (F), (I), and (K), error bars are 10–90 percentile, box is upper and lower quartiles, and center line is median. See also Figure S1.

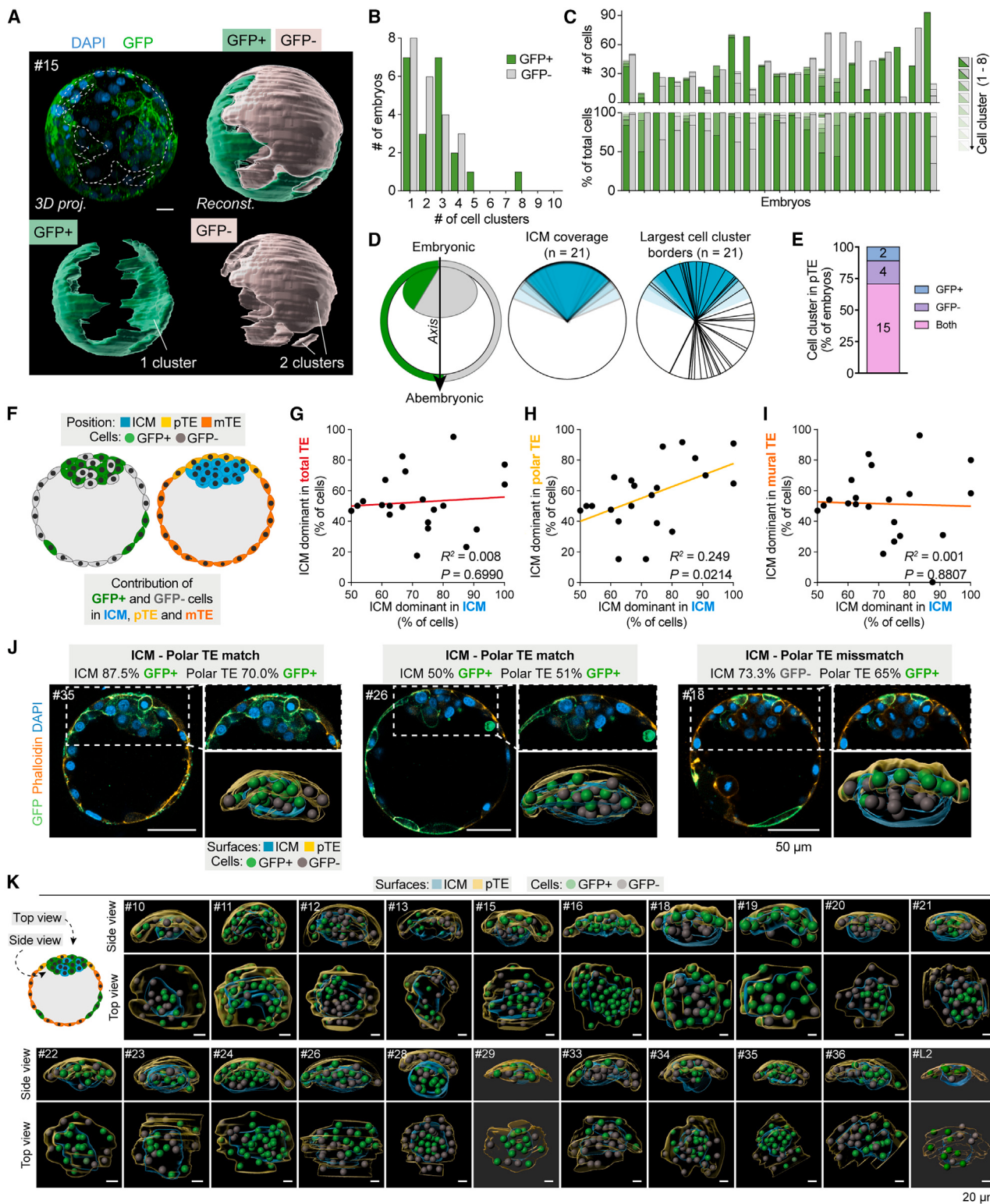


Figure 2. The ICM-dominant blastomere is enriched in the polar TE

(A) Quantification performed in (B)–(E). 3D blastocyst expressing GFP and stained with DAPI. Dotted white line delimits position of GFP- cells in TE. Reconstructions show shape and position of GFP+ and GFP- clusters. Scale bar, 50 μ m.

(legend continued on next page)

represented 71.25% of ICM cells, represented 49.36% of the TE (38.7 ± 19 cells) (Figure 1I). These clonal imbalances were independent of the embryo size (Figures S1M–S1P) and embryo quality (Figure S1E). Importantly, we found that within the ICM, one 2-cell blastomere generated an average of 76% of EPI cells (average 9 ± 4.1 out of 12 ± 5.3 EPI cells) and 53.7% of HYPO cells (average 2.5 ± 1.4 out of 5.2 ± 3 HYPO cells) (Figures 1J–1L).

In the TE, most embryos displayed 1–3 cell clusters of GFP+ or GFP– cells (Figures 2A–2C), with the largest clusters spreading along the embryonic-abembryonic axis (running meridionally from the pole having ICM to the opposite pole of the blastocyst, Figures 2D, 2E, and S2A). Thus, cells derived from each 2-cell blastomere contributed to both polar TE (overlying the ICM) and mural TE (covering the ICM-free blastocoel, Figure 2E). Importantly, the clonal composition of the ICM did not correlate with that of the mural TE or the whole TE but did positively correlate with the polar TE composition (Figures 2F–2K).

Taken together, we detect imbalances in the contribution of a 2-cell blastomere to the ICM versus TE and to the EPI versus HYPO within the ICM.

2-cell clonal imbalance is not explained by blastomere arrest or genomic instability

To investigate how this lineage bias arises, we first examined parameters of embryo quality. We observed large, mitotically arrested blastomeres in 8/22 blastocysts (36.4%) (Figure 3A), whose size suggested they arrested at the 4- or 8-cell stage, while the remaining blastomeres progressed in development. However, there was no clear correlation between clonal composition of the TE or ICM and the rate of blastomere arrest (Figure 3B), indicating that blastomere arrest does not underpin the observed clonal imbalances. We also measured the rate of blastomere arrest in embryos generated by *in vitro* fertilization (IVF) and recorded with the Embryoscope in the IVF clinic (STAR Methods). We observed that 15 out of 88 such embryos (17%) also had cells arresting around the 8-cell stage (Figures 3C and 3D).

Many human embryos are thought to contain aneuploid blastomeres, which could lead to miscarriage or congenital defects.^{30–33} In mouse embryo models of mosaic aneuploidy, aneuploid clones can be cleared from the ICM but survive in the TE, albeit with proliferative defects.^{34,35} Whether a similar clearing mechanism exists in the human embryo remains contested,^{36,37} but its existence has been suggested to explain line-

age allocation biases in the early embryo.^{1,38} Time-lapse imaging of human embryos revealed the presence of divisions with “lagging chromosomes,” a hallmark of chromosomal instability.^{32,33} In these blastomeres, chromosome separation at anaphase was incomplete and resulted in cytoplasmic DNA (cytDNA) clusters (Figure S4A). On average, we observed cytDNA in 8.1% of cells of the 22 blastocysts. CytDNA appeared at similar rates in both GFP+ and GFP– cells, as well as ICM and TE cells, and the proportion of cytDNA-containing cells was no different between embryos having different degrees of 2-cell clonal asymmetry (Figures 3E–3H). This suggests that chromosome instability is not a primary driver of the observed clonal imbalances.

Given that ICM clonal composition correlated with the polar but not mural TE (Figures 2H and 2I), we aimed to identify potential karyotypic differences correlating with the clonal imbalances we observed. We isolated ICM and polar TE from mural TE for sequencing (Figure 3I). Of 20 embryos sequenced, 2 gave partially inconclusive results; 14 were completely euploid; 2 were completely aneuploid; and 2 were aneuploid only in the ICM and polar TE (Figures 3J and S3A). Overall, only a small subset of the analyzed embryos had aneuploidies suggesting that clonal imbalances are independent of karyotypic aberrations.

Together with internal quality controls (Figures 1 and S1), these results argue against a primary role for blastomere arrest and aneuploidy in modulating the clonal composition of the blastocyst.

Live imaging reveals that asymmetric cell divisions at the 8-cell stage predict ICM composition

In the mouse, ICM cells are allocated through three successive rounds of ACD from the 8- to the 64-cell stages. The first wave of ACD at the 8- to 16-cell transition is biased toward generating EPI cells, whereas the second and third waves generate primitive endoderm (equivalent to human HYPO).^{8,9} ACD dynamics in the 8-cell-stage human embryo are poorly understood, and clonal imbalances in ICM cell allocation could be important in controlling ICM and EPI composition. To monitor ACD in human embryos, we used membrane-permeable fluorescent dyes to track genomic DNA (SPY555-DNA) and F-actin (SiR-actin) in live imaging experiments (Figure 4A). As a proof-of-concept, we recovered 2-cell mouse embryos from pregnant females, stained them, and imaged them until the blastocyst stage (Figures 4A and S4B). The cell cycle durations and rate of progression to the blastocyst stage were similar in stained and unstained mouse embryos (Figures 4B and S4C). In addition, SiR-actin

(B) Number of GFP+ or GFP– cell clusters/embryo in TE.

(C) Number (top) or percentage (bottom) of cells that compose each cell cluster, per embryo, shown by diminishing tones of color. Green: GFP+ clusters; gray: GFP– clusters. Each cluster (1–8) is ordered by size (cluster 1, largest).

(D) (Left) Embryonic-abembryonic axis in blastocyst. (Middle) Area covered by ICM in each embryo. (Right) Border separating the largest GFP+ and GFP– cell clusters in TE.

(E) Presence of the largest GFP+ and GFP– clusters in polar TE. Values indicate number of embryos.

(F) Schematic depicting quantifications performed in (G)–(I).

(G–I) Contribution of ICM-dominant population to ICM versus total TE (G), polar TE (H), or mural TE (I). R^2 and p value against a line with a zero-slope displayed.

(J) Human blastocysts expressing GFP and stained with DAPI and AF647-phalloidin, corresponding to quantifications shown in (H). ICM and polar TE (pTE) magnifications are displayed in each panel as fluorescence image (top) or reconstruction (bottom). Scale bars, 50 μ m.

(K) Reconstructions of ICM and polar TE. Dots are cells, colored by GFP expression. Top and side views presented. Scale bars, 20 μ m.

For (B)–(D) and (G)–(I), $n = 21$ human blastocysts. One embryo was excluded from the analysis (see STAR Methods).

See also Figure S2.

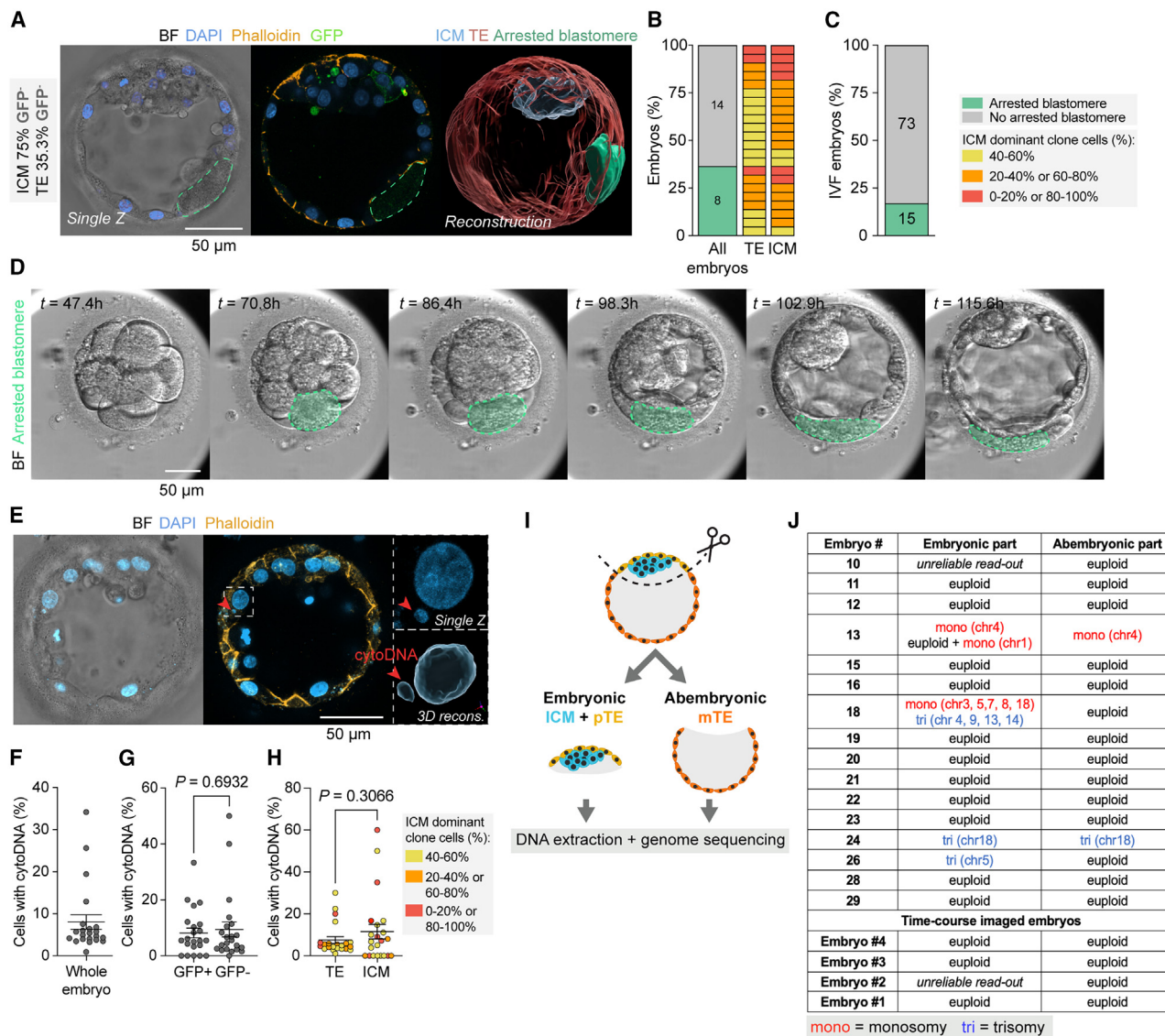


Figure 3. 2-cell clonal imbalance is not explained by blastomere arrest or genomic instability

(A) Human blastocyst with an arrested blastomere on TE surface. Blastocysts mosaic for GFP stained with AF647-phalloidin and DAPI. (Right) Reconstructions of TE, ICM, and arrested blastomere. Scale bar, 50 µm.

(B) Number of arrested blastomeres measured ($n = 22$ blastocysts). Side bars indicate degree of clonal imbalance in ICM or TE.

(C and D) Quantification and representative frames of a time-course imaging (D) depicting emergence of arrested blastomere in 8-cell-stage embryo. (C) $n = 88$ embryos. Scale bar, 50 µm.

For (B) and (C), numbers indicate embryo number.

(E) Human blastocyst with cell containing cytoDNA (arrowheads). Scale bars, 50 µm.

(F–H) Cells with cytoDNA in the whole embryo (F), GFP+ or GFP– cells (G), TE, or ICM (H). For (H), dots colored by clonal imbalance in ICM or TE. $n = 22$ blastocysts. Center lines are mean, and error bars are standard error. Statistical significance: t test.

(I) Schematic of protocol.

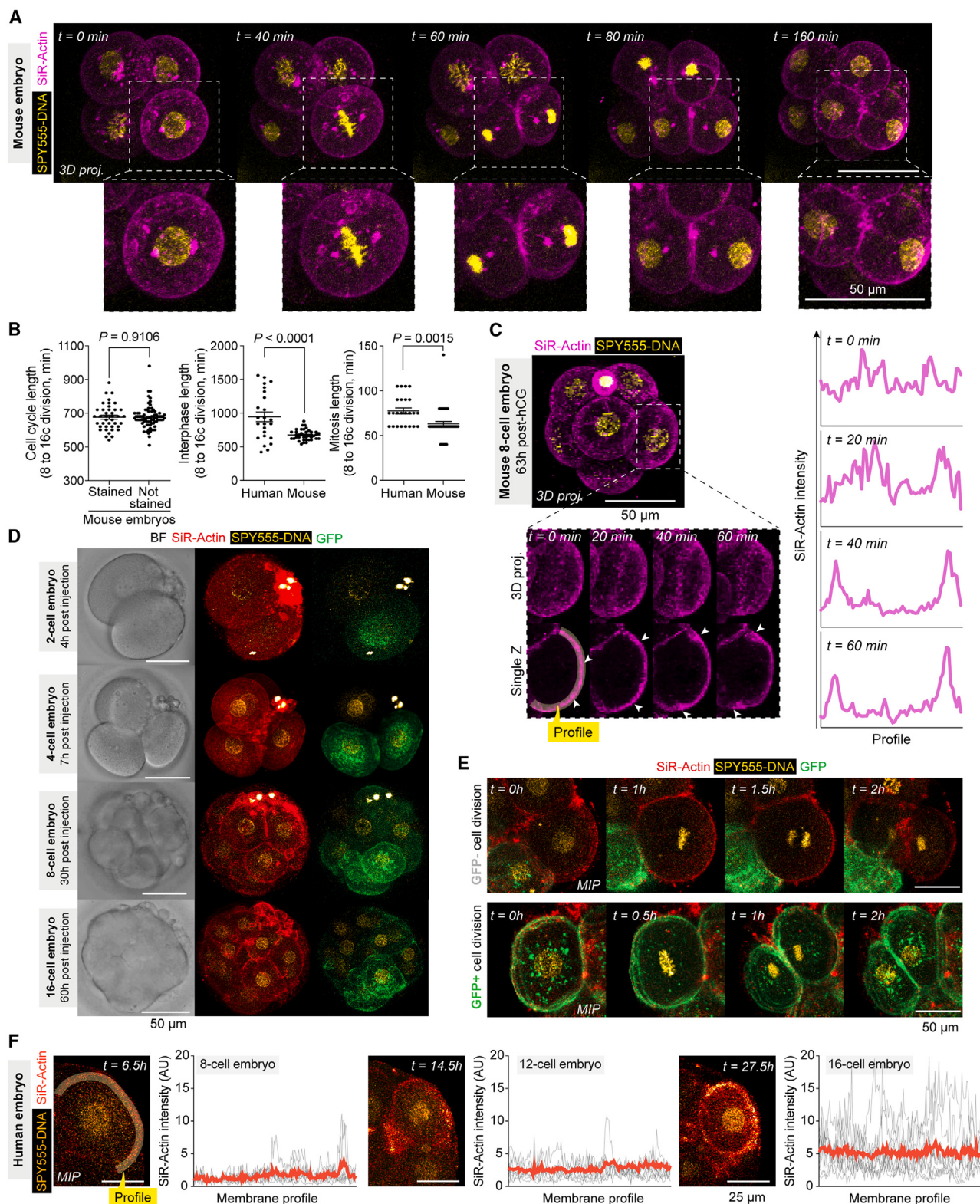
(J) Results of the sequencing ($n = 20$ embryos). Two embryos could not be included due to unavailability of the material for the analysis.

See also Figure S3.

staining allowed us to quantify the formation of the cortical F-actin ring in the apical region of 8-cell-stage blastomeres (Figure 4C).

We then applied our live embryo labeling protocol to a subset of mGap43-GFP-injected human embryos (Figures 4D and 4E). Nuclear and membrane co-labeling allowed us to follow com-

plete mitotic progression in GFP+ and GFP– human cells (Figure 4E). Compared with mouse 8-cell blastomeres, human 8-cell blastomeres had a longer interphase (15.75 h in human, 11.24 h in mouse) and mitosis (Figure 4B). We also observed the enrichment of cortical F-actin during 8- to 16-cell polarization of human embryos (Figure 4F). Thus, this labeling approach



(legend on next page)

allowed detailed capture of morphogenetic events by 3D confocal, time-lapse imaging.

To evaluate ACD at the 8- to 16-cell transition, we stained embryos with SiR-actin and SPY555-DNA at 27 h post-injection and imaged them for a further 28 h (Figures 5A and 5B). We tracked the position and division of each cell over time (Figure S5). We defined a division as ACD if it led to the ingression of one daughter cell to allocate an ICM cell (Figures 5A, 5C, and 5D, blue cell). By contrast, symmetric cell divisions (SCDs) had both daughter cells remaining at the embryo surface (Figures 5A, 5C, and 5D, red cell). We verified ACD and SCD by measuring the angle of division of the cells (Figure 5C). We observed a total of 28 divisions in the 4 embryos (Figure 5D). ACDs were less frequent than SCDs (Figures 5C and 5D), consistent with observations in mice.^{8,10,11} Importantly, the clonal composition of the ACD strongly predicted the clonal composition of the ICM at the blastocyst stage (Figures 5D and 5E). For instance, in embryo #4, three GFP– cells underwent ACD, and the blastocyst ICM was completely occupied by GFP– cells (Figures 5F and 5G). By contrast, in embryo #1, one GFP+ and one GFP– underwent ACD, and GFP+ cells represented 60% of the cells in the blastocyst ICM (Figure S5A). In embryo #2, we detected one GFP+ cell undergoing ACD when the embryo had only seven cells, and 75% of blastocyst ICM cells expressed GFP (Figure S5B). Although limited by the small sample size, our results suggest that early cell ingression is a strong predictor of ICM clonal composition.

A computational model of three parameters predicts clonal imbalance in human blastocysts

To test parameters that could explain the observed clonal composition in human embryos, we developed a statistical model of blastocyst development that predicts cell distributions through computer simulations. The model generated pools of 22 embryos, each with the total number of cells observed in our human blastocysts, but varying proportions of ICM and TE, averaging 17.4% of embryo cells in the ICM. Each modeled embryo started at the 2-cell stage with one blastomere randomly marked by GFP expression and followed embryo development through successive rounds of divisions. The expression of GFP (or lack thereof) was inherited by the daughter cells (Figure 6A).

First, we modulated three parameters that could affect the clonal composition of the human blastocysts: cell death, cell arrest, and ACD (Figure 6A). Based on literature,^{39–42} our model

stipulated that death randomly affected any embryo cell from the 64-cell stage onward, at an average rate of $p_{\text{death}} = 4.4\%$. This resulted in an average of 7%–8% dead cells per blastocyst (see below; Figure S6A), consistent with Brison.⁴² We calculated a cell arrest rate (p_{arrest}) of 6.5% affecting any cell at the 4- or 8-cell stage regardless of its clonal identity (Figures S6B and S6C; STAR Methods). These assumptions, which are consistent with previous reports,⁴³ resulted in a final blastocyst pool with the same proportion of embryos with arrested blastomeres as the one we had measured in our original sample (Figures 3B and S6D).

Finally, our model stipulated that each embryo underwent three consecutive waves of ACD, similar to the mouse embryo.⁸ Based on calculations from our embryo dataset, we estimated that the number of ACD in each wave, n_{inter} , varied uniformly in the ranges of 1–3, 1–2, and 0–1 cells per wave, respectively (Figures S6E and S6F; STAR Methods). Interestingly, these values are lower than those measured in mouse,⁸ but similar to those estimated in human embryos.⁴⁴ Modulating the number of internalization waves (Figure S6F) or the number of ACD in each wave (Figures S6E and S6G) showed that our design was the best at recapitulating the values measured in our blastocysts.

We randomly picked GFP+ and GFP– cells for internalization during these cleavage cycles, a choice we refer to as “unbiased” fate determination. For this process to represent both SCD and ACD, only up to one of two sister cells was allowed to be selected for internalization. In the mouse embryo, the number of cell internalizations is compensated across the internalization waves to balance the final number of ICM cells: if too few cells are internalized in the first wave, a higher number of cells will be internalized in the subsequent wave.^{15,45} To model this tendency, we mimicked this effect by automatically adjusting n_{inter} by the difference between the expected number of internalized cells and that accumulated over previous waves. From the 64-cell stage onward, the ICM and the TE were modeled to divide separately, until the final embryo size was reached.

Using these parameters through 10^4 repetitions predicted 220,000 embryos with distributions of GFP+/GFP– cells in the whole embryo that were not statistically different from the distributions observed in human blastocysts (Figures 6B and 6C, red). The model corroborated that GFP expression does not affect the developmental potential of injected blastomeres (as both modeled and real embryos had a similar distribution of GFP+ cells, Figures 6B and 6C) and reproduced the observed

Figure 4. Non-invasive labeling of human embryos

- (A) Mouse 4-cell-stage blastomere stained with SPY555-DNA and SiR-actin. Scale bars, 50 μm .
- (B) 8-to-16-cell transition: (left) cell-cycle length (min) in mouse embryos stained with SPY555-DNA and SiR-actin, or not stained ($N = 32$ cells, $n = 4$ embryos). (Middle) Interphase length in mouse and human embryos. (Right) Mitosis length in mouse and human embryos. For all plots center line is mean, error bars are standard error. For (B) statistical significance: t test. Mouse quantification ($N = 42$ cells, $n = 6$ embryos), human quantification ($N = 24$ cells, $n = 4$ embryos).
- (C) Representative images and quantification of apical F-actin ring progression in 8-cell-stage mouse blastomeres, stained with SPY555-DNA and SiR-actin. Scale bar, 50 μm , highlighted band: quantification profile; arrowheads: edges of ring.
- (D) Human embryos expressing mGap43-GFP in some cells stained with SiR-actin and SPY555-DNA and imaged at different time points. Scale bars, 50 μm . Embryos displayed at the 2-cell and 4-cell stage are not the 4 embryos included in Figure 5.
- (E) Representative images of GFP– (top) and GFP+ (bottom) human blastomeres dividing. Scale bars, 50 μm .
- (F) Representative frames and quantification of polarization process in human embryos. SiR-actin intensity in the membrane quantified across time. Gray lines are quantifications of the cortex of each cell in the embryo displayed, red line is average. Scale bars, 25 μm .
- In (A), (D), (E), and (F), zona pellucida was digitally removed during image processing.

See also Figure S4.

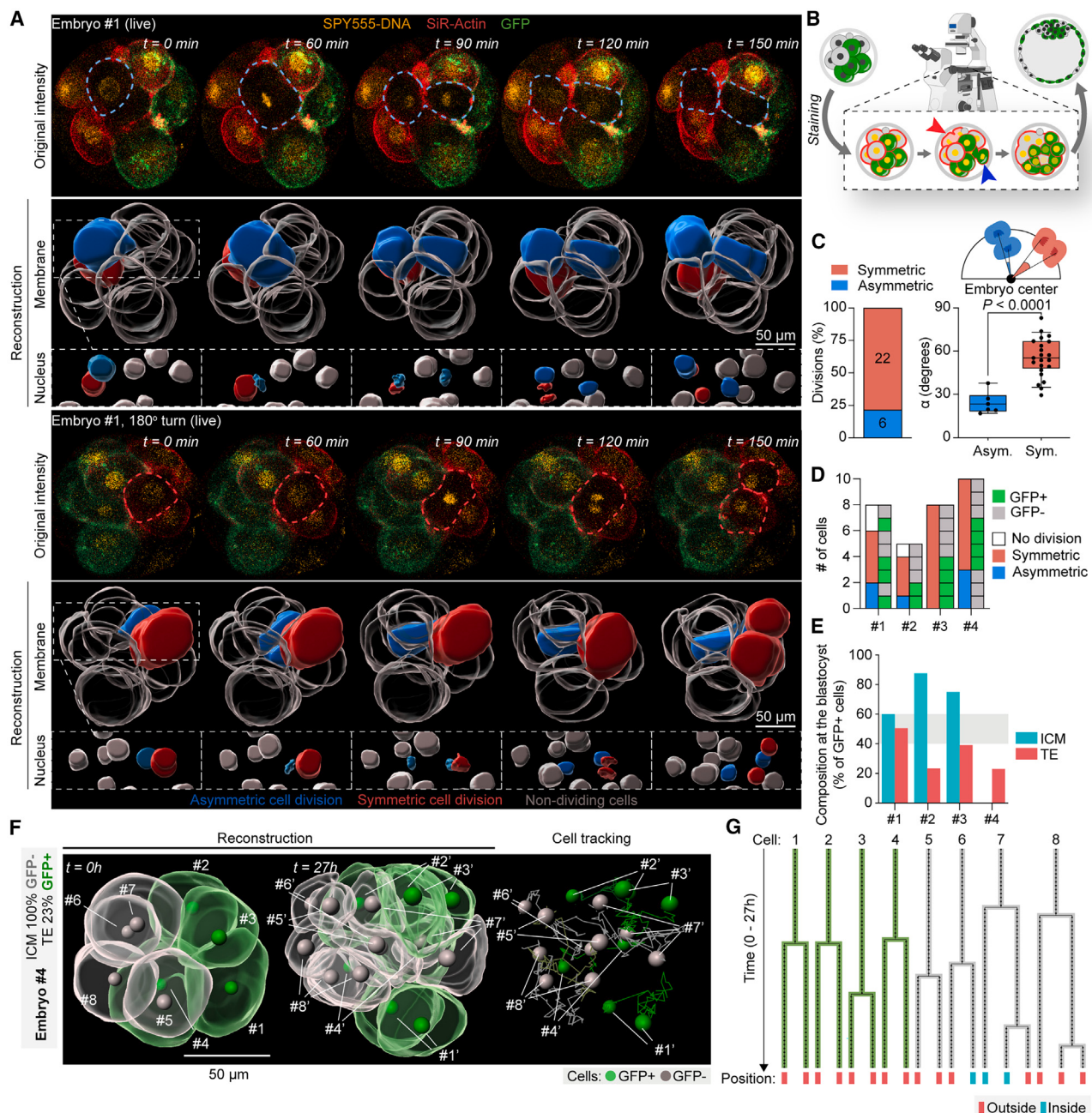


Figure 5. Live imaging of human embryos reveals that asymmetric cell division at the 8-cell stage predicts ICM clonal composition

(A) Asymmetric (top, blue) and symmetric (bottom, red) cell divisions in the same human embryo during 8-to-16-cell transition. Embryos mosaic for GFP stained with SIR-actin and SPY555-DNA at 8-cell stage and imaged over time. Zona was digitally removed for clarity. Scale bars, 50 µm.

(B) Schematic of embryo imaging using membrane-permeable dyes. Blue and red arrowheads indicate asymmetric and symmetric cell divisions, respectively.

(C) Proportion (left) and vectorial angle (right) of asymmetric and symmetric divisions. Right error bars: 10–90 percentile, box: upper and lower quartiles, and center line: median. Statistical significance: t test. $N = 28$ cells, $n = 4$ embryos. Two cells (one GFP+ and one GFP−) in embryo #1, and one cell (GFP−) in embryo #2 did not divide. Values are absolute number of cells.

(D) Number and type (GFP+ or GFP−) of cells with asymmetric or symmetric divisions, or not dividing.

(E) GFP+ cells in ICM or TE at the blastocyst stage. $n = 4$ human embryos.

(F and G) Example embryo tracked from the 8- to 16-cell stages. Scale bar, 50 µm.

See also Figure S5.

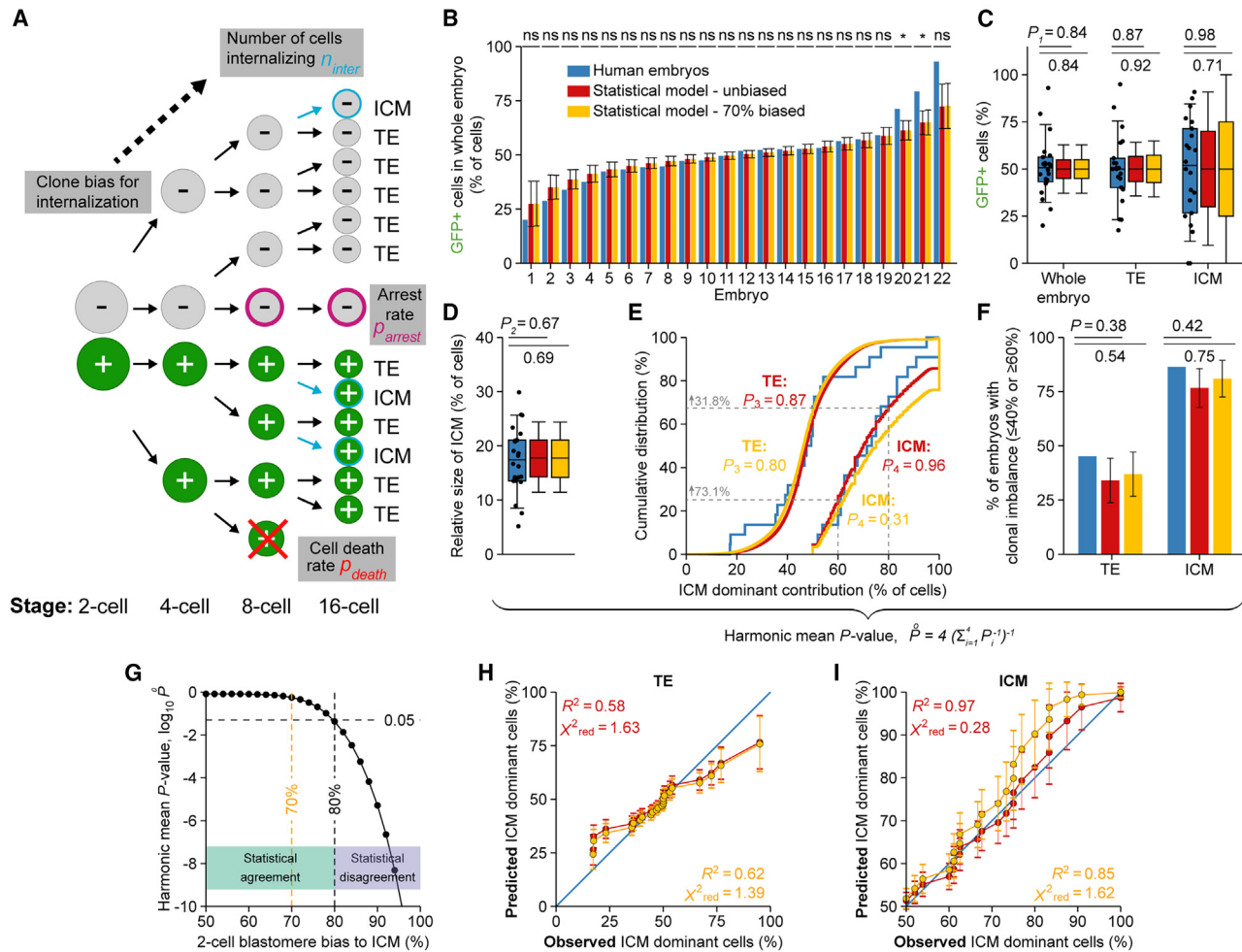


Figure 6. A computational model of three parameters predicts the clonal imbalance in human blastocysts

- (A) Schematic of the model. p_{death} : death rate, p_{arrest} : arrest rate, n_{inter} : number of cells internalizing in each division from 8- to 64-cell stages. n_{inter} is modulated to include a bias for ACD by one clone.
- (B) Observed (blue) and statistically predicted (unbiased, red; biased, yellow) distributions of GFP+ cells in 22 blastocysts. Predictions in (B), (F), (H), and (I) are mean \pm SD from 10^4 statistically independent realizations of 22 blastocysts. Random p_{arrest} as in Figure S6B (6.5%) and random p_{death} in ICM 4.4% from the 64-cell stage. p values in (B) (evaluated directly from the data) are $p > 0.05$ (ns) or $p < 0.05$ (*).
- (C) Distributions of GFP+ cells as in (B), by compartment. In (C) and (D) error bars: 10–90 percentile, box: upper and lower quartiles, and center line: median. p values in (C)–(F) are from two-sample Kolmogorov-Smirnov tests.
- (D) Relative size of the ICM as percent of embryo cells.
- (E) ICM-dominant contributions in TE and ICM. Gray dashed lines and small gray numbers indicate proportion of embryos with ICM-dominant contributions in the ICM $\geq 60\%$ or $\geq 80\%$ with “unbiased” model.
- (F) Embryos with ICM-dominant contribution $\geq 60\%$ in ICM, or $\geq 60\% - \leq 40\%$ in TE.
- (G) Overall statistical consistency between data and model, measured by harmonic mean of four p values from (C) (whole embryo), (D)–(F), as a function of the 2-cell clonal fate bias to become ICM. At $\sim 80:20$ bias, $\bar{P} = 0.05$ threshold is crossed. A 70:30 bias was chosen to represent the biased case (yellow) in (B)–(F), (H), and (I), as it is statistically representative without being a statistical edge case.
- (H and I) P-P plots showing predicted versus observed fraction of ICM-dominant cells in TE and ICM. Each point represents one of 22 blastocysts with statistical mean μ_i and SDs σ_i as error bars. R^2 is the coefficient of determination. $\chi^2_{\text{red}} = \frac{1}{22} \sum_{i=1}^{22} \left(\frac{x_i - \mu_i}{\sigma_i} \right)^2$ is the reduced chi-squared test statistic, which is low in absence of statistical disagreement.
- See also Figure S6.

distribution of ICM sizes (Figure 6D) as well as the clonal composition of TE and ICM (Figures 6E, 6H, and 6I). This model predicted a proportion of embryos with clonal imbalances in the TE and ICM that was statistically consistent with our measurements in blastocysts, albeit with lower frequencies (Figure 6F,

red bars). Quantitatively, the cumulative distribution (Figure 6E) predicted $\sim 73.1\%$ of embryos with $\geq 60\%$ of ICM cells from one 2-cell blastomere and $\sim 31.8\%$ of embryos with $\geq 80\%$ of ICM cells from one 2-cell blastomere. By assessing lineage compositions in 220,000 embryos modeled with minimal parameters,

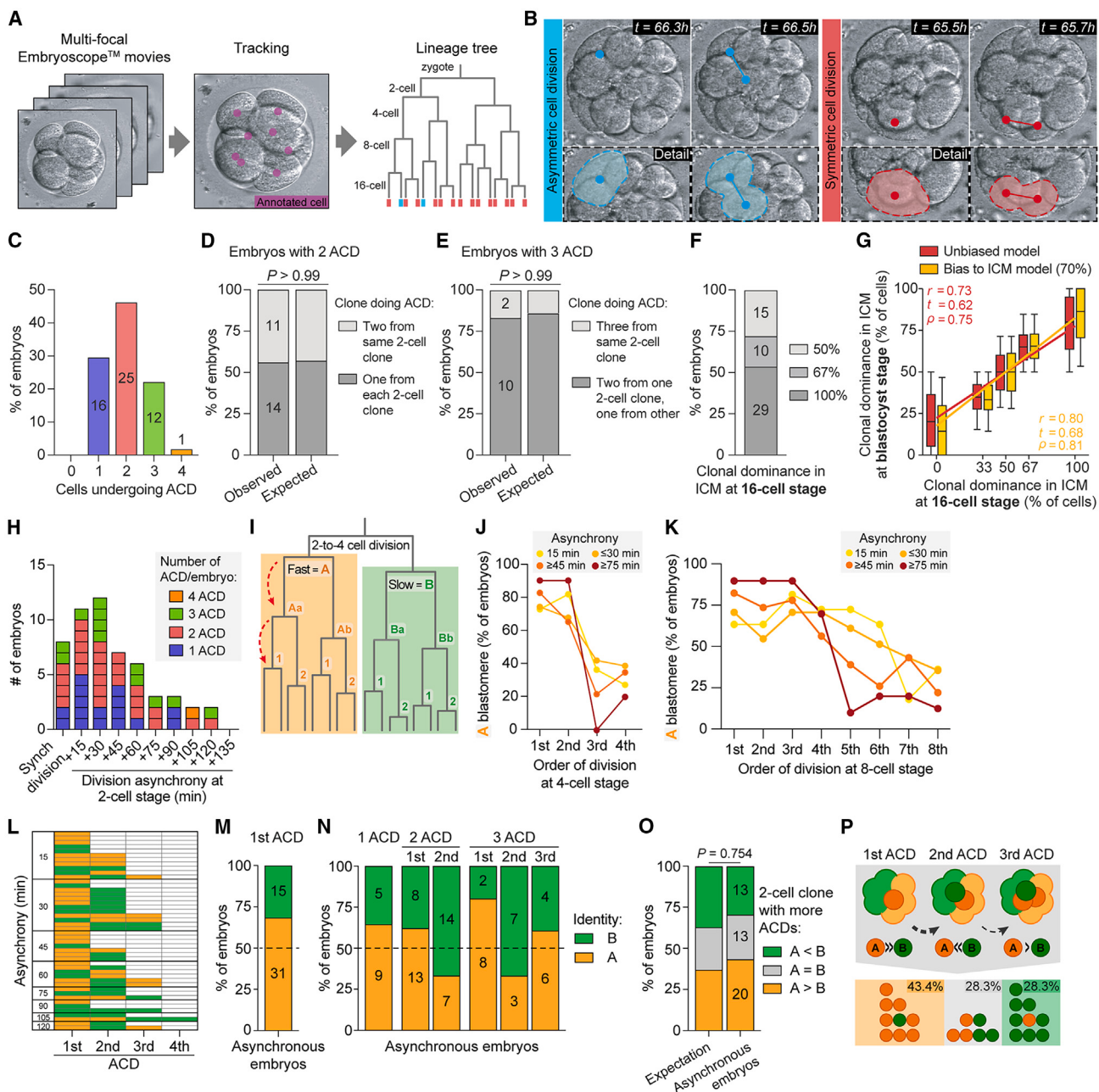


Figure 7. Lineage tracing reveals that faster-dividing blastomere in the 2-cell human embryo is biased toward the first ACD at the 8-cell stage
(A) Pipeline of the analysis.

(B) Asymmetric (inside-outside, left, blue) and symmetric (outside-inside, right panel, red) cell divisions in the same human embryo during the 8-to-16-cell transition, tracked in multifocal Embryoscope movie. t : absolute time provided with the embryoscope movie.

(C) Human embryos with different numbers of ACDs during 8-to-16-cell division. $n = 54$ embryos.

(D) Embryos with 2 ACDs from the same or different 2-cell clones during 8-to-16-cell division. Observed value was compared with value expected by combinatorial chance (see STAR Methods) using chi-squared test. $n = 25$ embryos.

(E) Embryos with 3 ACDs from same or different 2-cell clones during 8-to-16-cell division. Observed value was compared with value expected by combinatorial chance using chi-squared test. $n = 12$ embryos.

(F) 16-cell-stage human embryos with different levels of clonal dominance in ICM. $n = 54$ embryos.

(G) Correlation between clonal dominance in ICM at 16-cell and blastocyst stages. Data were extracted from the model presented in Figure 6. Modeled embryos with clonal compositions matching the ones reported in (F) were chosen, and their ICM composition at the blastocyst stage was recorded. Red: unbiased model,

(legend continued on next page)

the model validates our observations that in most embryos, the human ICM is clonally imbalanced and largely populated by one 2-cell clone. Overall, the model predicts that modulation of cell death, cell arrest, and ACD result in a distribution of embryos that will have clonally imbalanced ICMs.

Lineage tracing of time-lapse movies reveals clonal imbalances at the 8-to-16-cell division in human embryos

To extend our observations of ACD from live imaging (Figure 5), we analyzed multifocal, time-course bright-field movies of human embryos developing from zygote to the blastocyst stage in the IVF clinic with Embryoscope (Figures 7A and S7A; STAR Methods). Multifocal image quality was sufficient to manually track the lineage history of 54 embryos (STAR Methods). This resulted in a lineage tree for each embryo, in which we registered the timing of division of each blastomere at 2-, 4-, and 8-cell stage, as well as the clonal origin of each cell.

Similar to our live imaging analysis using dyes (Figure 4), we scored 8-cell blastomere divisions as SCD if they resulted in two daughter cells that remained outside, or as ACD if one of the daughters ingressed to form the emerging ICM (Figures 7B and S7B). In most of the 8-cell embryos analyzed (53/54; 98.1%), we observed between one and three ACDs, and in one embryo, four cells had ACDs (Figure 7C). These numbers are consistent with our previous observations (Figures 5C and 5D; Zhu et al.⁴⁴) and the number of ACDs used in our statistical model (Figures S6E–S6G). Interestingly, these numbers are lower than those in mice at the same stage, which show 2.84 ACD/embryo on average at the 8- to 16-cell transition.⁸ By contrast, human embryos had a lower average of 1.96 ACD/embryo at the same stage.

In 8-cell embryos with one ACD (16/54 embryos, 29.6%) or three ACDs (12/54, 22.2%), the ICM composition at the 16-cell stage was, by definition, clonally imbalanced. In 3.7% of embryos (2/54), all three ICM cells originated from the same 2-cell clone (Figure 7E). In embryos with two ACDs (25/54, 46.3%), ~44% of embryos (11/25) had ICM cells that originated from the same 2-cell blastomere and had a clonally imbalanced ICM (Figure 7D). The distribution of ACDs measured in the whole population revealed a majority of embryos (39/54, 72.2%) with unbal-

anced ICM founder cell allocation at the 16-cell stage (Figure 7F). Notably, 29/54 (53.7%) 16-cell-stage human embryos had inside cells that were derived completely from just one of the two 2-cell blastomeres.

We considered that successive rounds of ACDs at the 16- to 32- and 32- to 64-cell transitions could potentially restore clonal balance to the ICM. Cell compaction at the 16-cell stage (after which individual blastomeres could not be accurately followed in the Embryoscope movies) precluded us from tracing cells further. Our mathematical model incorporates this possibility, so we used it to project how different “starting” degrees of clonal imbalance at the 16-cell stage would be predicted to affect the composition of the ICM at the blastocyst stage. Interestingly, early clonal imbalances in ICM founder cells were largely inherited to the blastocyst stage, with only a ~12% chance for the original imbalance to be either neutralized or reversed (Figure 7G). Also, the clonal composition of the embryos imaged by Embryoscope (projected at the blastocyst stage) was statistically consistent with the clonal distributions measured in the TE and ICM of the embryos labeled at the 2-cell stage and analyzed at the blastocyst stage (Figure S7C). These results cross-validate our original observations with an independent dataset. Together, these data suggest that a low number of ACDs at the 8- to 16-cell transition leads to a large clonal imbalance in the ICM.

The faster-dividing 2-cell stage blastomere is biased toward the first ACD at the 8-cell stage

In mice, the 2-cell stage blastomere that divides first is reported to contribute more cells to the ICM and polar TE, whereas the blastomere that divides later gives rise to more cells of the mural TE.^{12,13,46} This led us to ask whether such a connection between division asynchrony at the 2-cell stage and ACD at the 8- to 16-cell transition exists in human embryo development.

Most embryos analyzed (46/54, 85.2%) exhibited asynchronous divisions at the 2- to 4-cell transition, with one blastomere (labeled “A”) dividing 15–120 min faster than the other (labeled “B,” Figure 7H). Division asynchrony was inherited through to the 4- and 8-cell stages, with daughter cells of the faster blastomere also dividing faster at these stages (Figures 7I–7K).

To investigate the relationship between clonal identity, division time, and ACD, we examined asynchronous embryos (Figure 7L).

yellow: model with a clonal fate bias to become ICM at 70%. Error bars: 10–90 percentile, box: upper and lower quartiles, and center line: median. Pearson’s *r*, Kendall’s τ , and Spearman’s ρ are specified. The lines are linear least-squares fits.

(H) Human embryos with different degrees of asynchrony at the 2-to-4-cell division and number of ACD per embryo. $n = 54$ embryos.

(I) Classification of 2-cell stage blastomeres as fast (“A”) or slow (“B”) according to their order of division at the 2-to-4-cell stage. Progeny of the “A” blastomere also divides faster at the 4- and 8-cell stages (red dashed arrows).

(J and K) Cells dividing in 1st–4th position with “A” (Aa or Ab) identity during 4-to-8-cell division (J) and cells dividing in 1st–8th position with “A” (Aa1 or 2, or Ab1 or 2) identity during 8-to-16-cell division in embryos with different degrees of asynchrony at the 2-cell stage. $n = 46$ embryos. In (J)–(P), synchronous embryos ($n = 8$) were excluded as “A” and “B” blastomeres could not be identified.

(L) Number and identity of ACDs during 8-to-16-cell division originating from the faster (“A”) or slower (“B”) clone.

(M) Embryos with first ACD coming either from “A” or “B” clone. $n = 46$ embryos. Dashed line indicates 50% of embryos.

(N) Embryos with ACD by the “A” or “B” blastomere. Embryos were separated by their total number of ACDs (1, $n = 14$; 2, $n = 21$; or 3, $n = 10$). For embryos with 2 or 3 ACD, quantification broken down by division order.

(O) Embryos at 16-cell stage containing more inner cells from “A” or “B,” or with the same number of inner cells from each clone. Observed value was compared with value expected by combinatorial chance and compared using a binomial test for [A=B] versus !(A=B) cases.

(P) Schematic of the results in (L)–(O).

For all panels, numbers in columns indicate the embryo number. For (K), (L), (N), and (O), $n = 46$ human embryos.

See also Figure S7.

In 31/46 embryos (67.4%), the first ACD originated from the faster “A” 2-cell blastomere (Figure 7M). In embryos with more than one ACD, the second ACD was mostly from the “B” blastomere (21/31; 67.7%). In embryos with three ACD, the third ACD was by the “A” blastomere in 6/10 embryos (Figure 7N).

In total, 43.5% of the asynchronous embryos analyzed (20/46) contained more “A” cells than “B” (Figure 7O), whereas only 28.3% of embryos (13/46) contained more “B” cells than “A” cells in their ICM (Figure 7O). In the remaining 13/46 (28.3%) embryos, ICM founders at the 16-cell stage were clonally balanced, with as many “A” cells as “B” (Figure 7O). These results suggest that the blastomere that divides first at the 2-cell stage is biased to contribute more ICM founder cells at the 16-cell stage (Figures 7P and S7D).

To determine if this bias would affect the clonal composition of the blastocyst, we returned to our mathematical model. We applied a fourth parameter that “biased” one 2-cell clone toward having more ACDs. Blastomeres were still randomly selected for internalization at the same total numbers but with unequal probability for GFP+ and GFP– clones. We found that a lineage bias of between 50% and 80% resulted in a model that was statistically consistent with the observed data (Figure 6G).

We repeated our simulations using a 70% bias and compared the clonal imbalances in the predicted embryos with our observations in the real human embryos. The percentage of GFP+ cells in the whole blastocyst, the size of the ICM, and the clonal distributions in the TE and ICM in the predicted embryos showed statistical agreement with the data from the real embryos (Figures 6B–6E). Importantly, the 70% bias in this model improved the inheritance of clonal imbalances in the ICM from the 16-cell stage to the blastocyst stage (Figure 7G), and the fraction of embryos with a clonally imbalanced TE or ICM more closely mimicked the observed data (Figure 6F).

Overall, our data suggest that the cell that divides faster at the 2- to 4-cell transition generates more of the very few inside cells in the initial wave and therefore contributes more to the ICM in the human blastocyst.

DISCUSSION

Retrospective construction of developmental cell lineages in humans predicted that the majority of the body might be derived from just one blastomere of the 2-cell embryo.^{1–5,47} But whether this is so, and the mechanisms remained unclear. Here, we used prospective lineage tracing, imaging of live human embryos, and mathematical modeling to track the fate of each of the 2-cell human blastomeres. We demonstrate that human 2-cell blastomeres contribute unequally to the ICM and polar TE, with one blastomere contributing a majority of EPI cells that will form the body. We show that this clonal imbalance is linked with the first 2-cell blastomere to divide being biased to contribute more inside cells, generating the small number of founding EPI cells.

On average, 71.25% of ICM cells originate from one 2-cell blastomere: although in most embryos (19 out of 22), one 2-cell blastomere contributed ≥60% of ICM cells, the 2-cell clonal contributions to the ICM ranged from near equal (~50% for 3/22 embryos) to fully biased (100% for 2/22 embryos). By contrast, the 2-cell clonal composition of the TE is more

balanced, with approximately half the embryos containing comparable numbers of cells from each 2-cell clone in their TE. These findings provide embryological validation of previous results suggesting a universal unequal contribution of early embryonic cells to the human body.^{1–5,47} Remarkably, the range of clonal imbalance we report matches the one predicted in these publications.

Our results support the hypothesis that clonal imbalances established during the earliest stages of our development affect the final lineage composition even though the precise lineage commitment of the 2-cell blastomeres is not deterministic.^{23,48} Imbalances in clonal composition can arise when ICM first forms at the 8-to-16-cell division. An uneven number of cells becoming internalized or an even number of internalized cells that have the same clonal identity generates a clonal imbalance. Importantly, however, the extent of the clonal imbalance decreases with the number of cells internalized: one internalized cell generates 100% imbalance, two internalized cells generate 100% bias close to half the time, three internalized cells generate 100% imbalance 16% of the time, etc. Together with our previous work,⁸ we observe a substantially lower number of cells becoming internalized during the 8-to-16-cell division in human compared to mouse embryos. In mouse embryos dividing from 8-to-16-cell stage, 21% had one internalized cell; 26%, two; 21%, three; 11%, four; and 21%, five.⁸ By contrast, in humans, the same transition showed that 30% had one internalized cell; 46%, two; 22%, three; and 2%, four. Others have also noted that the inner cell number at the morula stage and the ICM size at the blastocyst stage are larger in mouse than in human embryos.⁴⁹ This lower distribution of cells becoming internalized during the 8-to-16-cell division in human embryos anticipates a higher likelihood of clonal imbalance when compared with mouse. It will be of interest to decipher how the number of internalized cells is regulated in different mammalian species and the impact on development and clonal composition of the body.

We also explored how the topographical distribution of clones in the TE connects with asymmetries in composition of the ICM. 2-cell clones were organized in coherent TE cell clusters, indicating little cell mixing at the 8-to-32-cell stages, similar to mice.¹⁵ In mouse embryos, zygotic division along the animal-vegetal axis results in one 2-cell blastomere showing a biased contribution to the cells of the embryonic half of the embryo (the EPI and the overlaying polar TE), and the other forming the abembryonic mural TE and surface ICM cells that contribute more to the primitive endoderm.^{12,50} However, in humans, the largest cell cluster for each clone spread along the embryonic-abembryonic axis, resulting in the presence of cells from both clones in the polar TE. Despite this, and similarly to the mouse embryo, the 2-cell clonal composition in the human polar TE correlates with the clonal composition of the EPI. Differences and similarities in the mechanisms that self-organize human and mouse embryos include differences in the temporal sequence of morphogenetic events.^{6,25,44,49,51} Further exploration of these events will prove invaluable for understanding mechanisms for building the human embryo.

Genomic instability and aneuploidy have been suggested as drivers of asymmetric 2-cell clonal contribution in the human embryo.^{1,38} We show that most embryos used in this research were euploid, and the few aneuploid embryos present exhibited

ranging 2-cell clonal bias to the ICM and the TE. This suggests that genomic instabilities were not a primary cause for biased lineage allocations and that our dataset was composed of healthy human embryos. Moreover, a minority of embryos that implant and give rise to healthy births contain aneuploid cells, and most aneuploid embryos are postulated to be lost during pregnancy.^{33,52} Therefore, asymmetric clonal distributions detected in human adults^{1–3} are likely not a result of embryonic aneuploidy. This is further supported by our lineage tracing of embryos imaged with Embryoscope, which ultimately gave rise to a healthy birth while also exhibited clonal imbalances in their founding ICM population at the 16-cell stage. We infer that imbalanced lineage allocation reflects intrinsic developmental trajectories occurring in developing human embryos.

Several reports suggest that biased cell fate allocation in mouse embryos traces back to the cleavage division of the zygote,⁵⁰ resulting in asymmetries in the 2-cell embryo that are maintained and amplified in further cleavage divisions.^{13,15–19,23,50,53} At the 8-cell stage, the cells derived from one of these two mouse blastomeres have a higher number of ACDs and thus make a greater contribution to the ICM.¹⁵ Our lineage tracing of healthy embryos from the 2- to 16-cell stage revealed that the first 2-cell blastomere to divide had a higher propensity for the first ACD in its descendants. In these 16-cell embryos, only 28% had a clonally balanced cell population inside. The faster-dividing 2-cell blastomere dominated the population in 61% of the remaining embryos. Although mathematical modeling demonstrates that the observed clonal imbalance of the ICM can emerge from blastomeres that randomly divide asymmetrically, it suggests that a lineage bias for ACD of up to 80:20 for each clone remains statistically plausible. To what extent 2-cell asymmetries impact the clonal imbalance will require additional research, and our results suggest cooperation between stochastic and biasing mechanisms controlling the clonal makeup of the human embryo.

Our results point to the 8-to-16-cell transition as a bottleneck that predefines the composition of the ICM and EPI. We previously demonstrated in mouse embryos that cells from earlier asymmetric divisions exhibit greater plasticity in fate, contributing to the EPI.^{8,9} By contrast, cells from later waves were biased toward becoming the primitive endoderm rather than the EPI. The scarcity of the human zygotes available for research barred deeper exploration of subsequent waves of ACD after the 8–16 cell transition and the potential roles of other molecular and morpho-kinetic factors, such as zygote cleavage orientation,^{12,13,50,54} aneuploidies originating from the first mitotic division, or other asymmetric cellular dynamics at the early stages, before the 8-to-16-cell division.⁵⁵

Overall, our work shows that the human blastocyst is clonally imbalanced, with the majority of the EPI cells, and therefore the future body, originating from one blastomere at the 2-cell stage. Our results do not suggest a deterministic start of life in the human embryo. Rather, we propose that early bottlenecks of few ACDs at the 8-cell embryo stage lead to overrepresentation of descendants of one 2-cell blastomere in the ICM. Moreover, our data suggest that asynchronous cell division of the 2-cell blastomeres influence the ultimate lineage composition. Whether these asymmetries are adapted to promote successful development remains unexplored.

Limitations of the study

A major challenge in this study was the scarcity of embryos at the zygote stage. Donated research-consented embryos can only be sourced from IVF clinics, and zygote freezing is no longer a common clinical practice since embryos are now cultured to the blastocyst stage before freezing. The pool of zygote-stage human embryos available for research is therefore extremely limited. We circumvented this limitation by tracing the lineage of the 2-cell blastomeres from a larger collection of multi-plane bright-field Embryoscope time-lapse movies. Lineage contribution cannot be accurately tracked beyond the 16-cell stage due to embryo compaction. Finally, we use a statistical model to bypass sample size limits. In the model, we adjust the parameters following the best estimates available and/or by using our own data. Future studies characterizing the cellular dynamics of human development may help optimize the parameters and outputs of the model.

STAR★METHODS

Detailed methods are provided in the online version of this paper and include the following:

- [KEY RESOURCES TABLE](#)
- [RESOURCE AVAILABILITY](#)
 - Lead contact
 - Materials availability
 - Data and code availability
- [EXPERIMENTAL MODEL AND STUDY PARTICIPANT DETAILS](#)
 - Mouse embryo recovery and culture
 - Human embryo recovery and culture
 - Embryoscope™ time-lapse movies
- [METHOD DETAILS](#)
 - Microinjection of mGap43-GFP mRNA for cell and lineage labelling
 - Fixation and staining
 - Live staining with SIR-Actin and SPY555-DNA dyes
 - Time-lapse live imaging
 - Human blastocyst ploidy analysis
- [QUANTIFICATION AND STATISTICAL ANALYSIS](#)
 - Embryo exclusion criteria
 - Number of GFP+ and GFP- cells in the human blastocysts
 - Scoring of blastocysts using the Gardner and Schoolcraft blastocyst grading system
 - 3D projections of human blastocysts
 - Lineage tracing of the human embryo
 - Angle of cell division
 - Number, position and borders of clone clusters in trophectoderm
 - Clonal composition of the polar vs mural TE
 - Cell cycle length
 - Lineage tree reconstructions from 1- to 16-cell stage using Embryoscope™ time-lapse movies
 - Detection of the presence of arrested blastomeres
 - Statistical model of blastocyst development with random cell arrest, death and internalization

SUPPLEMENTAL INFORMATION

Supplemental information can be found online at <https://doi.org/10.1016/j.cell.2024.04.029>.

ACKNOWLEDGMENTS

We thank the patients who volunteered embryos for this work. We thank María Luisa Pardinas, María José De los Santos Molina, and IVIRMA Valencia for

securing access to Embryoscope movies; Mingshu Liao and Changhuei Yang for help on image preparation; and David Glover, Adiyant Lamba, and Angela Andersen for invaluable advice. Some drawings were adapted from BioRender ([BioRender.com](https://biorender.com)). This work was supported by the Human Science Frontiers Program (LT0022/2022-L to S.J.), the NOMIS Foundation (12540449 to M.Z.-G.), the Wellcome Trust (207415/Z/17/Z to M.Z.-G.), the Open Philanthropy Project (to M.Z.-G.), the Shuri & Kay Curci Foundation (to M.Z.-G.), and the Weston Havens Foundation (to M.Z.-G.).

AUTHOR CONTRIBUTIONS

Conceptualization: S.J., M.M., and M.Z.-G.; methodology: S.J., M.M., and R.V.; software: R.V. and D.I.; formal analysis: S.J., M.M., C.K., E.M.P., L.I.-S., and R.V.; investigation: S.J., M.M., L.I.-S., and D.-Y.C.; resources: R.M., P.R., R.J.P., and M.Z.-G.; writing: S.J., M.M., and M.Z.-G.; visualization: S.J. and M.M.; supervision: D.I. and M.Z.-G.; funding acquisition: S.J., N.A., D.I., and M.Z.-G.

DECLARATION OF INTERESTS

N.A. is the founder and CEO of Progenesis Inc.

Received: May 4, 2023

Revised: December 6, 2023

Accepted: April 22, 2024

Published: May 13, 2024

REFERENCES

- Cooren, T.H.H., Oliver, T.R.W., Sanghvi, R., Sovio, U., Cook, E., Vento-Tormo, R., Haniffa, M., Young, M.D., Rahbari, R., Sebire, N., et al. (2021). Inherent mosaicism and extensive mutation of human placentas. *Nature* 592, 80–85. <https://doi.org/10.1038/s41586-021-03345-1>.
- Cooren, T.H.H., Moore, L., Robinson, P.S., Sanghvi, R., Christopher, J., Hewinson, J., Przybillka, M.J., Lawson, A.R.J., Spencer Chapman, M., Cagan, A., et al. (2021). Extensive phylogenies of human development inferred from somatic mutations. *Nature* 597, 387–392. <https://doi.org/10.1038/s41586-021-03790-y>.
- Fasching, L., Jang, Y., Tomasi, S., Schreiner, J., Tomasini, L., Brady, M.V., Bae, T., Sarangi, V., Vasmatzis, N., Wang, Y., et al. (2021). Early developmental asymmetries in cell lineage trees in living individuals. *Science* 371, 1245–1248. <https://doi.org/10.1126/science.abe0981>.
- Park, S., Mali, N.M., Kim, R., Choi, J.W., Lee, J., Lim, J., Park, J.M., Park, J.W., Kim, D., Kim, T., et al. (2021). Clonal dynamics in early human embryogenesis inferred from somatic mutation. *Nature* 597, 393–397. <https://doi.org/10.1038/s41586-021-03786-8>.
- Spencer Chapman, M., Ranzoni, A.M., Myers, B., Williams, N., Cooren, T.H.H., Mitchell, E., Butler, T., Dawson, K.J., Hooks, Y., Moore, L., et al. (2021). Lineage tracing of human development through somatic mutations. *Nature* 595, 85–90. <https://doi.org/10.1038/s41586-021-03548-6>.
- Molè, M.A., Weberling, A., and Zernicka-Goetz, M. (2020). Comparative analysis of human and mouse development: From zygote to pre-gastrulation. In *Current Topics in Developmental Biology*, 136 (Academic Press Inc.), pp. 113–138. <https://doi.org/10.1016/bs.ctdb.2019.10.002>.
- Zhu, M., and Zernicka-Goetz, M. (2020). Principles of Self-Organization of the Mammalian Embryo. *Cell* 183, 1467–1478. <https://doi.org/10.1016/J.CELL.2020.11.003>.
- Morris, S.A., Teo, R.T.Y., Li, H., Robson, P., Glover, D.M., and Zernicka-Goetz, M. (2010). Origin and formation of the first two distinct cell types of the inner cell mass in the mouse embryo. *Proc. Natl. Acad. Sci. USA* 107, 6364–6369. <https://doi.org/10.1073/pnas.0915063107>.
- Morris, S.A., Graham, S.J.L., Jedrusik, A., and Zernicka-Goetz, M. (2013). The differential response to Fgf signalling in cells internalized at different times influences lineage segregation in preimplantation mouse embryos. *Open Biol.* 3, 130104. <https://doi.org/10.1098/RSOB.130104>.
- Johnson, M.H., and Ziomek, C.A. (1981). The foundation of two distinct cell lineages within the mouse morula. *Cell* 24, 71–80. [https://doi.org/10.1016/0092-8674\(81\)90502-X](https://doi.org/10.1016/0092-8674(81)90502-X).
- Fleming, T.P. (1987). A quantitative analysis of cell allocation to trophectoderm and inner cell mass in the mouse blastocyst. *Dev. Biol.* 119, 520–531. [https://doi.org/10.1016/0012-1606\(87\)90055-8](https://doi.org/10.1016/0012-1606(87)90055-8).
- Piotrowska, K., Wianny, F., Pedersen, R.A., and Zernicka-Goetz, M. (2001). Blastomeres arising from the first cleavage division have distinguishable fates in normal mouse development. *Development* 128, 3739–3748. <https://doi.org/10.1242/dev.128.19.3739>.
- Piotrowska-Nitsche, K., Pereira-Gomez, A., Haraguchi, S., and Zernicka-Goetz, M. (2005). Four-cell stage mouse blastomeres have different developmental properties. *Development* 132, 479–490. <https://doi.org/10.1242/dev.01602>.
- Dietrich, J.E., and Hiiragi, T. (2007). Stochastic patterning in the mouse pre-implantation embryo. *Development* 134, 4219–4231. <https://doi.org/10.1242/DEV.003798>.
- Bischoff, M., Parfitt, D.E., and Zernicka-Goetz, M. (2008). Formation of the embryonic-abembryonic axis of the mouse blastocyst: Relationships between orientation of early cleavage divisions and pattern of symmetric/asymmetric divisions. *Development* 135, 953–962. <https://doi.org/10.1242/dev.014316>.
- Goolam, M., Scialdone, A., Graham, S.J.L., MacAulay, I.C., Jedrusik, A., Hupalowska, A., Voet, T., Marioni, J.C., and Zernicka-Goetz, M. (2016). Heterogeneity in Oct4 and Sox2 Targets Biases Cell Fate in 4-Cell Mouse Embryos. *Cell* 165, 61–74. <https://doi.org/10.1016/j.cell.2016.01.047>.
- Torres-Padilla, M.E., Parfitt, D.E., Kouzarides, T., and Zernicka-Goetz, M. (2007). Histone arginine methylation regulates pluripotency in the early mouse embryo. *Nature* 445, 214–218. <https://doi.org/10.1038/nature05458>.
- White, M.D., Angiolini, J.F., Alvarez, Y.D., Kaur, G., Zhao, Z.W., Mocskos, E., Bruno, L., Bissiere, S., Levi, V., and Plachta, N. (2016). Long-Lived Binding of Sox2 to DNA Predicts Cell Fate in the Four-Cell Mouse Embryo. *Cell* 165, 75–87. <https://doi.org/10.1016/j.cell.2016.02.032>.
- Sun, H., Su, J., Wu, T., Wang, F., Kang, J., Zhang, J., Xing, X., Cheng, Y., and Zhang, Y. (2020). CARM1 is heterogeneous in mouse four-cell embryo and important to blastocyst development. *Reproduction* 159, 91–104. <https://doi.org/10.1530/REP-19-0405>.
- Wang, J., Wang, L., Feng, G., Wang, Y., Li, Y., Li, X., Liu, C., Jiao, G., Huang, C., Shi, J., et al. (2018). Asymmetric Expression of LincGET Biases Cell Fate in Two-Cell Mouse Embryos. *Cell* 175, 1887–1901.e18. <https://doi.org/10.1016/j.cell.2018.11.039>.
- Panamarova, M., Cox, A., Wicher, K.B., Butler, R., Bulgakova, N., Jeon, S., Rosen, B., Seong, R.H., Skarnes, W., Crabtree, G., et al. (2016). The BAF chromatin remodelling complex is an epigenetic regulator of lineage specification in the early mouse embryo. *Development* 143, 1271–1283. <https://doi.org/10.1242/dev.131961>.
- Lim, H.Y.G., Alvarez, Y.D., Gasnier, M., Wang, Y., Tetlak, P., Bissiere, S., Wang, H., Biro, M., and Plachta, N. (2020). Keratins are asymmetrically inherited fate determinants in the mammalian embryo. *Nature* 585, 404–409. <https://doi.org/10.1038/s41586-020-2647-4>.
- Chen, Q., Shi, J., Tao, Y., and Zernicka-Goetz, M. (2018). Tracing the origin of heterogeneity and symmetry breaking in the early mammalian embryo. *Nat. Commun.* 9, 1819. <https://doi.org/10.1038/s41467-018-04155-2>.
- Lawrence, P.A., and Levine, M. (2006). Mosaic and regulative development: two faces of one coin. *Curr. Biol.* 16, R236–R239. <https://doi.org/10.1016/J.CUB.2006.03.016>.
- Regin, M., Essahib, W., Demtschenko, A., Dewandre, D., David, L., Gerri, C., Niakan, K., Verheyen, G., Tournaye, H., Sterckx, J., et al. (2023). Lineage segregation in human pre-implantation embryos is specified by YAP1 and TEAD1. *Hum. Reprod.* 38, 1484–1498. <https://doi.org/10.1101/2022.09.29.509946>.
- Roode, M., Blair, K., Snell, P., Elder, K., Marchant, S., Smith, A., and Nichols, J. (2012). Human hypoblast formation is not dependent on FGF

- signalling. *Dev. Biol.* 361, 358–363. <https://doi.org/10.1016/J.YDBIO.2011.10.030>.
27. Niakan, K.K., and Eggan, K. (2013). Analysis of human embryos from zygote to blastocyst reveals distinct gene expression patterns relative to the mouse. *Dev. Biol.* 375, 54–64. <https://doi.org/10.1016/J.YDBIO.2012.12.008>.
28. Kuijk, E.W., van Tol, L.T.A., van de Velde, H., Wubbolts, R., Welling, M., Geijsen, N., and Roelen, B.A.J. (2012). The roles of FGF and MAP kinase signaling in the segregation of the epiblast and hypoblast cell lineages in bovine and human embryos. *Development* 139, 871–882. <https://doi.org/10.1242/DEV.071688>.
29. Hardy, K., Handyside, A.H., and Winston, R.M.L. (1989). The human blastocyst: cell number, death and allocation during late preimplantation development in vitro. *Development* 107, 597–604. <https://doi.org/10.1242/DEV.107.3.597>.
30. van den Berg, M.M.J., van Maarle, M.C., van Wely, M., and Goddijn, M. (2012). Genetics of early miscarriage. *Biochim. Biophys. Acta* 1822, 1951–1959. <https://doi.org/10.1016/J.BBADIS.2012.07.001>.
31. Ljunger, E., Cnattingius, S., Lundin, C., and Anerén, G. (2005). Chromosomal anomalies in first-trimester miscarriages. *Acta Obstet. Gynecol. Scand.* 84, 1103–1107. <https://doi.org/10.1111/J.0001-6349.2005.00882.X>.
32. Strom, C.M., Ginsberg, N., Applebaum, M., Bozorgi, N., White, M., Caffarelli, M., and Verlinsky, Y. (1992). Analyses of 95 first-trimester spontaneous abortions by chorionic villus sampling and karyotype. *J. Assist. Reprod. Genet.* 9, 458–461. <https://doi.org/10.1007/BF01204052/METRICS>.
33. Martínez, M.C., Méndez, C., Ferro, J., Nicolás, M., Serra, V., and Landeras, J. (2010). Cytogenetic analysis of early nonviable pregnancies after assisted reproduction treatment. *Fertil. Steril.* 93, 289–292. <https://doi.org/10.1016/J.FERTNSTERT.2009.07.989>.
34. Singla, S., Iwamoto-Stohl, L.K., Zhu, M., and Zernicka-Goetz, M. (2020). Autophagy-mediated apoptosis eliminates aneuploid cells in a mouse model of chromosome mosaicism. *Nat. Commun.* 11, 2958. <https://doi.org/10.1038/s41467-020-16796-3>.
35. Bolton, H., Graham, S.J.L., Van Der Aa, N., Kumar, P., Theunis, K., Fernandez Gallardo, E., Voet, T., and Zernicka-Goetz, M. (2016). Mouse model of chromosome mosaicism reveals lineage-specific depletion of aneuploid cells and normal developmental potential. *Nat. Commun.* 7, 11165. <https://doi.org/10.1038/ncomms11165>.
36. Coticchio, G., Barrie, A., Lagalla, C., Borini, A., Fishel, S., Griffin, D., and Campbell, A. (2021). Plasticity of the human preimplantation embryo: Developmental dogmas, variations on themes and self-correction. *Hum. Reprod. Update* 27, 848–865. <https://doi.org/10.1093/humupd/dmab016>.
37. Yang, M., Rito, T., Metzger, J., Naftaly, J., Soman, R., Hu, J., Albertini, D.F., Barad, D.H., Brivanlou, A.H., and Gleicher, N. (2021). Depletion of aneuploid cells in human embryos and gastruloids. *Nat. Cell Biol.* 23, 314–321. <https://doi.org/10.1038/s41556-021-00660-7>.
38. Kalousek, D.K., and Dill, F.J. (1983). Chromosomal Mosaicism Confined to the Placenta in Human Conceptions. *Science* 221, 665–667. <https://doi.org/10.1126/SCIENCE.6867735>.
39. Regin, M., Lei, Y., De Deckersberg, E.C., Guns, Y., Verdyck, P., Verheyen, G., Van de Velde, H., Sermon, K., and Spits, C. (2023). Complex aneuploidy triggers autophagy and p53-mediated apoptosis and impairs the second lineage segregation in human preimplantation embryos. *eLife* 12, RP88916. <https://doi.org/10.7554/ELIFE.88916>.
40. Hardy, K. (1999). Apoptosis in the human embryo. *Rev. Reprod.* 4, 125–134. <https://doi.org/10.1530/REVREPROD/4.3.125>.
41. Hardy, K., Stark, J., and Winston, R.M.L. (2003). Maintenance of the Inner Cell Mass in Human Blastocysts from Fragmented Embryos. *Biol. Reprod.* 68, 1165–1169. <https://doi.org/10.1093/BIOLREPROD.102.010090>.
42. Brison, D.R. (2000). Apoptosis in mammalian preimplantation embryos: Regulation by survival factors. *Hum. Fertil. (Camb)* 3, 36–47. <https://doi.org/10.1080/1464727002000198671>.
43. Yang, S.H., Wu, C.H., Chen, Y.C., Yang, C.K., Wu, T.H., Chen, P.C., and Tsai, H.D. (2018). Effect of morphokinetics and morphological dynamics of cleavage stage on embryo developmental potential: A time-lapse study. *Taiwan. J. Obstet. Gynecol.* 57, 76–82. <https://doi.org/10.1016/J.TJOG.2017.12.013>.
44. Zhu, M., Shahbazi, M.N., Martin, A., Zhang, C., Sozen, B., Borsos, M., Mandelbaum, R.S., Paulson, R.J., Mole, M.A., Esbert, M., et al. (2021). Human embryo polarization requires plc signaling to mediate trophectoderm specification. *eLife* 10, e65068. <https://doi.org/10.7554/ELIFE.65068>.
45. Saiz, N., and Plusa, B. (2013). Early cell fate decisions in the mouse embryo. *Reproduction* 145, R65–R80. <https://doi.org/10.1530/REP-12-0381>.
46. Kelly, S.J., Mulnard, J.G., and Graham, C.F. (1978). Cell division and cell allocation in early mouse development. *J. Embryol. Exp. Morphol.* 48, 37–51.
47. Ju, Y.S., Martincorena, I., Gerstung, M., Petljak, M., Alexandrov, L.B., Rahbari, R., Wedge, D.C., Davies, H.R., Ramakrishna, M., Fullam, A., et al. (2017). Somatic mutations reveal asymmetric cellular dynamics in the early human embryo. *Nature* 543, 714–718. <https://doi.org/10.1038/nature21703>.
48. Van De Velde, H., Cauffman, G., Tournaye, H., Devroey, P., and Liebaers, I. (2008). The four blastomeres of a 4-cell stage human embryo are able to develop individually into blastocysts with inner cell mass and trophectoderm. *Hum. Reprod.* 23, 1742–1747. <https://doi.org/10.1093/HUMREP/DEN190>.
49. Gerri, C., McCarthy, A., Alanis-Lobato, G., Demtschenko, A., Bruneau, A., Loubersac, S., Fogarty, N.M.E., Hampshire, D., Elder, K., Snell, P., et al. (2020). Initiation of a conserved trophectoderm program in human, cow and mouse embryos. *Nature* 587, 443–447. <https://doi.org/10.1038/s41586-020-2759-x>.
50. Piotrowska, K., and Zernicka-Goetz, M. (2001). Role for sperm in spatial patterning of the early mouse embryo. *Nature* 409, 517–521. <https://doi.org/10.1038/35054069>.
51. Firmin, J., Ecker, N., Danon, D.R., Lange, V.B., Turlier, H., Patrat, C., and Maître, J.-L. (2022). Mechanics of human embryo compaction. Preprint at bioRxiv. <https://doi.org/10.1101/2022.01.09.475429>.
52. Rodriguez-Purata, J., Lee, J., Whitehouse, M., Moschini, R.M., Knopman, J., Duke, M., Sandler, B., and Copperman, A. (2015). Embryo selection versus natural selection: how do outcomes of comprehensive chromosome screening of blastocysts compare with the analysis of products of conception from early pregnancy loss (dilation and curettage) among an assisted reproductive technology population? *Fertil. Steril.* 104, 1460–66.e1. <https://doi.org/10.1016/J.FERTNSTERT.2015.08.007>.
53. Hupalowska, A., Jedrusik, A., Zhu, M., Bedford, M.T., Glover, D.M., and Zernicka-Goetz, M. (2018). CARM1 and Paraspeckles Regulate Pre-implantation Mouse Embryo Development. *Cell* 175, 1902–1916.e13. <https://doi.org/10.1016/j.cell.2018.11.027>.
54. Piotrowska-Nitsche, K., and Zernicka-Goetz, M. (2005). Spatial arrangement of individual 4-cell stage blastomeres and the order in which they are generated correlate with blastocyst pattern in the mouse embryo. *Mech. Dev.* 122, 487–500. <https://doi.org/10.1016/j.mod.2004.11.014>.
55. Currie, C.E., Ford, E., Benham Whyte, L., Taylor, D.M., Mihalas, B.P., Erent, M., Marston, A.L., Hartshorne, G.M., and McAinch, A.D. (2022). The first mitotic division of human embryos is highly error prone. *Nat. Commun.* 13, 6755. <https://doi.org/10.1038/s41467-022-34294-6>.
56. Borsos, M., Perricone, S.M., Schauer, T., Pontabry, J., de Luca, K.L., de Vries, S.S., Ruiz-Morales, E.R., Torres-Padilla, M.E., and Kind, J. (2019). Genome-lamina interactions are established de novo in the early mouse embryo. *Nature* 569, 729–733. <https://doi.org/10.1038/s41586-019-1233-0>.
57. Schindelin, J., Arganda-Carreras, I., Frise, E., Kaynig, V., Longair, M., Pietzsch, T., Preibisch, S., Rueden, C., Saalfeld, S., Schmid, B., et al. (2012). Fiji: an open-source platform for biological-image analysis. *Nat. Methods* 9, 676–682. <https://doi.org/10.1038/nmeth.2019>.
58. Ershov, D., Phan, M.S., Pylvänäinen, J.W., Rigaud, S.U., Le Blanc, L., Charles-Orszag, A., Conway, J.R.W., Laine, R.F., Roy, N.H., Bonazzi, D.,

- et al. (2022). TrackMate 7: integrating state-of-the-art segmentation algorithms into tracking pipelines. *Nat. Methods* 19, 829–832. <https://doi.org/10.1038/s41592-022-01507-1>.
59. Tinevez, J.Y., Perry, N., Schindelin, J., Hoopes, G.M., Reynolds, G.D., Laplantine, E., Bednarek, S.Y., Shorte, S.L., and Eliceiri, K.W. (2017). TrackMate: An open and extensible platform for single-particle tracking. *Methods* 115, 80–90. <https://doi.org/10.1016/J.YMETH.2016.09.016>.
 60. Thomas, M.R., Sparks, A.E., Ryan, G.L., and Van Voorhis, B.J. (2010). Clinical predictors of human blastocyst formation and pregnancy after extended embryo culture and transfer. *Fertil. Steril.* 94, 543–548. <https://doi.org/10.1016/J.FERTNSTERT.2009.03.051>.
 61. Zhu, M., Cornwall-Scoones, J., Wang, P., Handford, C.E., Na, J., Thomson, M., and Zernicka-Goetz, M. (2020). Developmental clock and mechanism of de novo polarization of the mouse embryo. *Science* 370, eabd2703. https://doi.org/10.1126/SCIENCE.ABD2703/SUPPL_FILE/ABD2703S9.MOV.
 62. Weber, R.J., Pedersen, R.A., Wianny, F., Evans, M.J., and Zernicka-Goetz, M. (1999). Polarity of the mouse embryo is anticipated before implantation. *Development* 126, 5591–5598. <https://doi.org/10.1242/DEV.126.24.5591>.
 63. Zernicka-Goetz, M., Pines, J., McLean Hunter, S.M.L., Dixon, J.P.C., Sieimering, K.R., Haseloff, J., and Evans, M.J. (1997). Following cell fate in the living mouse embryo. *Development* 124, 1133–1137. <https://doi.org/10.1242/DEV.124.6.1133>.
 64. Graham, S.J.L., Wicher, K.B., Jedrusik, A., Guo, G., Herath, W., Robson, P., and Zernicka-Goetz, M. (2014). BMP signalling regulates the pre-implantation development of extra-embryonic cell lineages in the mouse embryo. *Nat. Commun.* 5, 5667. <https://doi.org/10.1038/ncomms6667>.
 65. Virnicchi, G., Bora, P., Gahurova, L., Šušor, A., and Bruce, A.W. (2020). Wwc2 Is a Novel Cell Division Regulator During Preimplantation Mouse Embryo Lineage Formation and Oogenesis. *Front. Cell Dev. Biol.* 8, 857. <https://doi.org/10.3389/FCELL.2020.00857/BIBTEX>.
 66. Paim, L.M.G., and FitzHarris, G. (2022). Cell size and polarization determine cytokinesis furrow ingress dynamics in mouse embryos. *Proc. Natl. Acad. Sci. USA* 119, e2119381119. <https://doi.org/10.1073/PNAS.2119381119.SM01.AVI>.
 67. Anani, S., Bhat, S., Honma-Yamanaka, N., Krawchuk, D., and Yamanaka, Y. (2014). Initiation of Hippo signaling is linked to polarity rather than to cell position in the pre-implantation mouse embryo. *Development* 141, 2813–2824. <https://doi.org/10.1242/DEV.107276/VIDEO-2>.
 68. Domingo-Muelas, A., Skory, R.M., Moverley, A.A., Ardestani, G., Pomp, O., Rubio, C., Tetlak, P., Hernandez, B., Rhon-Calderon, E.A., Navarro-Sánchez, L., et al. (2023). Human embryo live imaging reveals nuclear DNA shedding during blastocyst expansion and biopsy. *Cell* 186, 3166–3181.e18. <https://doi.org/10.1016/J.CELL.2023.06.003>.
 69. Hardarson, T., Van Landuyt, L., and Jones, G. (2012). The blastocyst. *Hum. Reprod.* 27 (Suppl 1), i72–i91. <https://doi.org/10.1093/HUMREP/DES230>.

STAR★METHODS

KEY RESOURCES TABLE

REAGENT or RESOURCE	SOURCE	IDENTIFIER
Antibodies		
Goat anti-Sox17 primary antibody	R&D systems	Cat# AF1924; RRID: AB_355060
Donkey anti-Goat secondary antibody AlexaFluor 568	Thermo Fisher Scientific	Cat# A-11057; RRID: AB_2534104
Chemicals, peptides, and recombinant proteins		
M2 medium	Millipore-Sigma	M7167-100ML
EmbryoMax® Advanced KSOM Medium	Millipore-Sigma	MR-101-D
Mineral oil	Irvine Scientific	9305
Quinn's Advantage™ Embryo Thaw Kit	CooperSurgical	ART-8016
global® human embryo culture media	CooperSurgical	LGGG-050
Multipurpose Handling Medium-Complete (MHM-C) with Gentamicin	Irvine Scientific	90166
Alexa Fluor® 647 Phalloidin	ThermoFisher Scientific	A12381
DAPI	ThermoFisher Scientific	D3571
SiR-Actin	Cytoskeleton Inc.	CY-SC001
SPY555-DNA	Cytoskeleton Inc.	CY-SC201
NUCLEAR-ID Red DNA stain	Enzo	ENZ-52406
Acidic Tyrode's Solution	Millipore-Sigma	T1788
Critical commercial assays		
Human blastocyst ploidy analysis	Progenesis Inc. 4150 Regents Park Row, Suite 245 La Jolla CA 92037, USA	N/A
Experimental models: Organisms/strains		
B6SJLF1/J mice	The Jackson Laboratory	Cat# 100012; RRID: IMSR_JAX:100012
Human embryos	HRC Fertility Clinic 55 S. Lake Ave, 9th Fl. Pasadena CA 91101, USA	N/A
Recombinant DNA		
pRN3P_membrane_EGFP plasmid	Addgene, Borsos et al. ⁵⁶	Plasmid #139402; RRID: Addgene_139402
Software and algorithms		
Fiji (ImageJ)	Schindelin et al. ⁵⁷	https://fiji.sc/ ; RRID: SCR_002285
TrackMate plug-in for Fiji	Ershov et al. ⁵⁸ ; Tinevez et al. ⁵⁹	https://imagej.net/plugins/trackmate/
Imaris	Oxford Instruments	RRID: SCR_007370
MATLAB	The MathWorks, Inc.	http://www.mathworks.com/products/matlab/ RRID: SCR_001622
Custom MATLAB program	This study	supplemental information or https://git.bsse.ethz.ch/iber/Publications/2024_junyent-meglicki_blastomeres
Other		
PMSG	Prospec	HOR-272
hCG	Chorulon	031345
mMessage mMachine T3 kit	Thermo Fischer Scientific	AM1348
FemtoJet micro-injection pump	Eppendorf	FemtoJet
Negative capacitance	Electra 705	World Precision Instruments
Glass Bottom Dishes	MatTek Corporation	P35G-1.5-14-C
Ibidi Dishes	Ibidi	81158

RESOURCE AVAILABILITY

Lead contact

Further information and requests for resources and reagents should be directed to and will be fulfilled by the lead contact, Prof. Magdalena Zernicka-Goetz (maggdaz@caltech.edu).

Materials availability

This study did not generate new unique reagents. Specific reagents (e.g., plasmids) can be obtained on request after contacting the [lead contact](#).

Data and code availability

- All data reported in this paper will be shared by the [lead contact](#) upon request.
- All original code is available in this paper's [supplemental information](#).
- Any additional information required to reanalyze the data reported in this paper is available from the [lead contact](#) upon request.

EXPERIMENTAL MODEL AND STUDY PARTICIPANT DETAILS

Mouse embryo recovery and culture

Ethical approval for studies on mouse embryos was received from the Institutional Animal Care and Use Committee (IACUC) at the California Institute of Technology. To obtain mouse embryos at the 2-cell stage, 4-week-old B6S females (B6SJLF1/J) were stimulated to superovulate by intraperitoneal injection of pregnant mare serum gonadotrophin (PMSG; 10IU; Prospec, HOR-272) and, 48h later, intraperitoneal injection of human chorionic gonadotrophin (hCG; 10IU; Chorulon, 031345). Immediately after hCG injection, females were mated with B6S males. The females were sacrificed 45 hours post hCG to obtain 2-cell embryos. Oviducts were isolated in M2 medium (Millipore-Sigma, M7167-100ML) and cut into pieces with fine scissors. For longer culture, embryos were transferred to drops of preequilibrated EmbryoMax® Advanced KSOM Medium (Sigma, MR-101-D) and cultured in standard conditions (37°C, 5%CO₂) under mineral oil (Irvine Scientific, 9305).

Human embryo recovery and culture

Human embryo work was approved by the California Institute of Technology Committee for the Protection of Human Subjects (IRB protocol numbers 19-0948 and 22-0101, approved before the experiments were performed).

Human embryos at the zygote stage were obtained from HRC Fertility. Supernumerary cryopreserved embryos were donated after completion of IVF. They were not created for research purposes. Patients were informed of the conditions of the donation, objectives, and methodology of human embryo research. They were offered counselling and alternative options, including discarding embryos and continued cryopreservation. Patients were informed that they would not benefit directly from the donation of embryos to research. A total of 54 anonymized donated human embryos at the zygote two pronuclei stage (day 1 post-fertilization) were used. Embryos were thawed using Quinn's Advantage™ Embryo Thaw Kit (CooperSurgical, ART-8016) as per the manufacturer's instructions. Subsequently, the embryos were transferred to preequilibrated (overnight, 37°C, 5%CO₂) global® human embryo culture media (CooperSurgical, LGGG-050) and cultured in standard culture conditions (37°C, 5%CO₂) under mineral oil (Irvine Scientific, 9305) for 12-20h (~17h), until they reached 2-cell stage. Five embryos degenerated before the completion of the first zygotic division and could not be used for the study. Of the remaining 49 embryos, 29 developed to the blastocyst stage (Figure 1A). This ratio of successful *in vitro* human embryo culture is in line with previous reports.^{26,60}

The dataset obtained is unique, as access to human zygotes is extremely limited for several reasons: (1) research-consented embryos can only be sourced from IVF clinics and their availability relies on patient donation; (2) the practice of zygote freezing is no longer commonly used and the current practice is to culture embryos to the blastocyst stage, at which point assessments of embryo quality can be performed, and then frozen for subsequent IVF cycles. Thus, the pool of zygote stage embryos that is available for research is extremely limited and may be even smaller in the future. Embryos at other stages are unusable for the purpose of this study, as clonal origin cannot be identified for lineage prospective studies.

Embryoscope™ time-lapse movies

Embryoscope™ time-lapse movies of human embryos from the zygote to blastocyst stage were provided by IVIRMA-Valencia (IVI Foundation, Spain). These movies were generated during routine IVF clinical practice, when the embryos were placed in time-lapse incubators. The use of movies for retrospective analysis was approved by the Research Ethics Committee of IVI Valencia (IRB protocol number 2203-VLC-028-MD). Embryo imaging preceded the work presented in this manuscript, and this project had no impact on the culture practices of the embryos analyzed. The movies were anonymized before being received by the researchers. The IRB approval of the protocol 2203-VLC-028-MD stated that informed consent letters were "not applicable, as this is a retrospective study that carried out exclusively with anonymized or pseudonymized data". IRB approval ensured that the proposed project fulfilled the requirements of Organic Law 3/2018, of 5 December, on Personal Data Protection and guarantee of digital rights (Spain), Regulation

(EU) 2016/679 of the European Parliament and of the Council of 27 April 2016 on the protection of individuals with regard to the processing of personal data and on the free movement of such data, Law 14/2007, of 3 July, on Biomedical Research (Spain), Law 14/2006, of 26 May, on Assisted Reproduction Techniques (Spain), as well as the regulations that develop them. The California Institute of Technology Committee for the Protection of Human Subjects assessment of the use of these data in the retrospective analysis (application 21-1177) confirmed that the work was exempt of IRB approval as it represented secondary research for which consent is not required, as specified in the U.S. Federal Code (45 C.F.R. § 46.104).

METHOD DETAILS

Microinjection of mGap43-GFP mRNA for cell and lineage labelling

mRNA encoding a membrane targeting sequence of GAP43 fused with GFP (mGap43-GFP) was prepared by *in vitro* transcription (IVT) with the mMessage mMachine T3 kit (Thermo Fischer Scientific, AM1348) from linearized pRN3p plasmid containing mGap43-GFP (Plasmid #139402, Addgene)⁵⁶ sequence, as previously described.⁶¹ Briefly, the plasmid was linearized with SfiI restriction enzyme (Thermo Fischer Scientific, #FD1824) and purified with QIAquick PCR purification Kit (Qiagen, #28104). Subsequently, IVT was performed overnight (16h) with mMessage mMachine T3 kit according to the manufacturer's instructions, using 1 μg of the linearized template in the IVT reaction. Subsequently, synthesized mRNA was purified using lithium chloride precipitation included in the kit, according to the kit manufacturer instructions. The RNA was resuspended in 20 μL of Invitrogen™ Nuclease-Free Water (Thermo Fischer Scientific, #AM9937). Quality and quantity of the synthesized RNA was confirmed with Nanophotometer and by gel electrophoresis.

Human embryos at the 2-cell stage were transferred to Multipurpose Handling Medium-Complete (MHM-C) with Gentamicin (Irvine Scientific, 90166) for microinjection. One blastomere of each embryo, chosen at random, was injected with a minimal volume of 100 ng/μL of mGap43-GFP mRNA using a Femtojet micro-injection system (Eppendorf) with negative capacitance. We have previously shown that this method does not affect the developmental potential of mouse or human blastomeres.^{62,63} The technique of microinjection of mGap43-GFP mRNA for use as a neutral lineage tracing marker, in both mouse and human embryos, has been well reported.^{16,17,44,53,56,64–67} We verified the previously optimized⁴⁴ concentration of mGAP43-GFP in human embryos in a pilot experiment, ensuring that it would result in a clear membrane signal in all cells developing from the injected blastomere and that it would not affect the development of the embryo to the blastocyst stage. We reasoned that a membrane marker would enable annotation of the position and boundaries of cells in both the ICM and the TE. The embryo microinjection in all our experiments was performed by an expert, with over a decade of experience in micromanipulation of mammalian embryos. Furthermore, microinjection of human embryos had successfully been performed using the same system previously.⁴⁴ Following microinjection, embryos were transferred to fresh drops of preequilibrated (37°C, 5%CO₂) global® human embryo culture media under mineral oil for culture for 4 (to Day 5 of development) or 5 (to Day 6 of development) days, until the formation of an expanded blastocyst (at 37°C, 5%CO₂).

Fixation and staining

Embryos were fixed in freshly prepared 4% PFA in PBS for 20 min at room temperature (RT). Fixed embryos were washed twice in PBS without Mg²⁺/Ca²⁺ (PBS) containing 0.1% Tween-20 (PBST). Embryos were permeabilized in PBS containing 0.3% Triton X-100 and 0.1M Glycine for 20 min (RT) and incubated overnight (4°C) in PBST with Alexa Fluor® 647 Phalloidin (1:400, ThermoFisher Scientific, A12381) and DAPI (ThermoFisher Scientific, D3571) to visualize the F-actin cytoskeleton and nuclei, respectively. Subsequently, they were washed 3 times in PBST and 2 times in M2 medium and transferred to drops of M2 medium under mineral oil on glass-bottom dishes for imaging. Images were taken on a Leica SP8 confocal, using a 40x water immersion objective (N.A. = 1.10).

For immunostaining, embryos were washed 3 times in PBST and incubated in blocking buffer (PBST containing 1% fetal calf serum) for 1h (RT). Embryos were moved to blocking buffer containing Goat anti-SOX17 primary antibody (1:250, R&D systems, AF1924) overnight at 4°C and then washed in PBST (3 x 15 min) and incubated with secondary antibody (Donkey anti-Goat AF568, 1:1,000 in blocking buffer, ThermoFisher Scientific, A-11057) at RT for 2h. Subsequently, embryos were washed in PBST (3 x 5 min) and in drops of M2 medium (2 x 5 min) and moved to drops of M2 medium under mineral oil on glass-bottom dishes for imaging, as described above. Two embryos were unavailable for SOX17 staining and were excluded from the relevant figures.

Live staining with SiR-Actin and SPY555-DNA dyes

For live staining, human embryos were placed in 10-20 μL drops of preequilibrated global® human embryo culture media containing SiR-Actin (1 μM; Cytoskeleton Inc., CY-SC001) and SPY555-DNA (2X; Cytoskeleton Inc., CY-SC201) dyes. After 2h of incubation, embryos were transferred to small drops of the same medium containing both dyes at a lower concentration (100 nM SiR-Actin and 0.2X SPY555-DNA), under mineral oil, on μ-Dish 35 mm, high Glass Bottom dishes (Ibidi, 81158) for time-lapse live imaging.

To stain mouse embryos, the same steps were followed but the media used was EmbryoMax® Advanced KSOM, preequilibrated at 37°C, 5%CO₂.

Recent publications report the use of the same dyes in human embryos, at equivalent concentrations as the ones used in our study, without deleterious effects.^{55,68}

Time-lapse live imaging

For time-lapse live imaging, a Zeiss LSM980 confocal microscope equipped with a culture chamber module stabilized at 37°C, 5% CO₂ was used. Embryos were imaged with the following parameters: frequency: 30 min; 18 planes per stack; z-step: 5 µm; objective: 40x, objective N.A. = 1.2.

Human blastocyst ploidy analysis

Zona pellucida were removed from fixed blastocysts by treatment with Acidic Tyrode's Solution (Sigma, T1788), followed by three washes in M2 medium. The blastocysts were transferred to fresh drops of M2 medium and split with a tungsten wire needle into the embryonic part (ICM + polar TE) and abembryonic part (mural TE). Each resulting tissue/sample was washed separately through a fresh drop of ultrapure MiliQ water and collected in a PCR tube containing 5 µL H₂O. Subsequently, 1 µL of lysis buffer (200 mM KOH, 50 mM DTT in MiliQ H₂O) was added to each PCR tube. The samples were incubated at 65°C for 10 min. Following this, the samples were spun down and 1 µL of neutralization buffer (0.9 M Tris base pH 8.3, 0.3 M KCl, 0.2 M HCl in MiliQ H₂O) was added to each tube. The samples were stored at -20°C prior to the Pre-implantation Genetic Testing for Aneuploidy (PGT-A) analysis.

PGT-A analysis was performed by Progenesis Inc (La Jolla, CA) testing laboratory and a next-generation sequencing platform. Following cell lysis and DNA extraction, whole genome amplification was performed on the specimens using the ReproSeq™ PGS Kit. Amplified products were pooled to form the initial library and template enrichment was performed using the Ion Chef automated system. The library was finally loaded on a 540 chip for sequencing, using the Ion S5 XL Sequencing Kit (Life Technologies). There were an average of 150,000 to 200,000 reads and 200 base pairs per amplicon. Filtering for polyclonals was performed with Torrent SuiteTM software and then evaluated for aneuploidy using Ion Reporter™ software (Thermo Fisher Scientific). NGS plots were evaluated for chromosome copy number to determine both whole chromosome and segmental aneuploidies.

QUANTIFICATION AND STATISTICAL ANALYSIS

Embryo exclusion criteria

After fixation, imaging and initial characterization of the 29 embryos that developed to the blastocyst stage, 7 embryos were excluded from further analysis for the following reasons:

- Four embryos had an abundance of dead cells (both from the GFP+ and GFP- clone) that made it impossible to reliably quantify clonal contributions.
- Two embryos were completely GFP- and it was impossible to assess whether the initial injection had not been successful (no embryos with only GFP+ cells were observed).
- One embryo from the pilot trial had a very small ICM (4 cells).

All other embryos (n = 22) were used in all reported quantifications. Exceptionally, one or more embryos were excluded from one analysis for reasons particular to the measurements performed. These cases are detailed in the figure legends, and listed here:

- Two embryos from the test trial were not accessible for SOX17 staining and were excluded from the quantifications in [Figures 1K, S1H, and S1I](#). The sample size for these experiments is n = 20.
- Two embryos from the test trial were not accessible for DNA extraction and karyotyping and were excluded from [Figures 3J and S3](#). The sample size for these experiments is n = 20.
- One embryo was damaged during sample processing and was excluded from the topographical analyses in [Figures 2B–2I](#). The sample size for these experiments is n = 21.

Number of GFP+ and GFP- cells in the human blastocysts

Counting of GFP positive and negative cells in the ICM or TE was completed by 2 independent assessors in a blinded manner, using Fiji (ImageJ).⁵⁷ In the case of any discrepancies between these independent assessments, a third assessment was completed by the two assessors together to discuss reasons for the discrepancies and agree on the actual number of cells. GFP intensity was not a relevant measurement in the quantifications performed. Rather, the expression or absence of GFP in a cell was assessed. Therefore, small variations in the level of GFP expression did not have an influence on our results. After injection, mGAP43-GFP mRNA is expressed in the labelled cell and all of that cell's descendants throughout preimplantation development. We performed extensive internal controls ([Figures 1, 3, 6, and S1](#)) that demonstrate that microinjection did not have deleterious effects on the developmental potential of the labelled blastomere.

GFP+ and GFP- cell counts were used to quantify the clonal composition of the TE, ICM, EPI and HYPO, according to the contribution of either cell population to each compartment. The most abundant clone (>50% cells) in the ICM was labelled "ICM-dominant" and used as reference population in both the ICM and the TE. In one embryo, either the GFP+ clone or the GFP- clone could be ICM-dominant.

Scoring of blastocysts using the Gardner and Schoolcraft blastocyst grading system

Transmitted brightfield images of blastocysts were analyzed by two independent researchers to score their overall fitness using the Gardner and Schoolcraft blastocyst grading system.⁶⁹ This system uses a code of one number plus two letters to describe the expansion level of the blastocyst stage (number; 1 to 6), and the size and aspect of the ICM (first letter; A to C) and the TE (second letter; A to C). A combination of letter scores was used to assign a “Good”, “Fair” or “Poor” quality assessment to each embryo, following this grading: Good (AA, AB, BA), Fair (AC, BB), Poor (BC, CA, CB, CC).

3D projections of human blastocysts

Three-dimensional (3D) embryo projections were generated using Imaris software (Oxford Instruments). The “Spots” tool was used to generate a 3D map of the position (ICM or TE) and GFP expression (GFP+ or GFP-) of the cells in the blastocysts analyzed. Spots segmentation was semi-automated, based on DAPI expression, and corrected manually. Classes for position and GFP expression were assigned manually. The “Surface” tool was used to generate 3D volumetric reconstructions. Surface segmentation was performed manually and adapted to the requirements of each measurement (as displayed in the figures). For time-course movies, the membrane and nucleus of single cells at each frame were reconstructed in Imaris. Symmetric divisions were defined as divisions resulting in two cells that remained on the surface of the embryo; asymmetric divisions led to the ingress of one cell into the embryo. For time-course images, the zona pellucida was digitally subtracted from the image for clarity, as indicated in the figure legends.

Lineage tracing of the human embryo

Imaris was used to trace the position and lineage of each cell in the cleavage stage embryos imaged. The “Spots” tool was used to draw a spot at the center of each cell, using the SPY555-DNA signal as reference. Spots for each cell were linked throughout the movie to generate the lineage of that cell, including the time and position (XYZ coordinates) of cell divisions, and the final position of the cells after division. Cell classification, according to GFP expression (GFP+ and GFP-), as well as the final cell position in the embryo (inside or outside) was recorded.

Angle of cell division

For the four cleavage stage embryos imaged, cell division angle was measured using Imaris. For each cell division, at the time of cytokinesis, the X, Y and Z coordinates for the two daughter cells and for the geometric center of the embryo were annotated. The angle formed between the vectors connecting daughter 1-center of the embryo and daughter 2-center of the embryo was measured and used in the figures.

Number, position and borders of clone clusters in trophectoderm

Quantification of the number, position and size of the TE cell clusters was performed using Imaris software. The spot representations of the cells, as well as the actual Phalloidin signal (which reports cell borders) were used for the measurement. A cell cluster was defined as a single cell, or a group of cells of the same type (GFP+ or GFP-) that contacted each other and were fully bordered by cells of the other type. In most embryos, one larger cell cluster for each clone was apparent, containing most of the cells from that clone in the TE. Other smaller clusters were also present, often close to the edges separating the larger clusters from each clone. The number, size and position for each cluster in each blastocyst were recorded and post-processed, as presented in the figures. To describe the spatial organization of GFP+ and GFP- cell clusters, the larger cluster form each clone was used. Using Imaris software, embryos were positioned to place the ICM at the top of the image and the line separating the largest GFP+ and GFP- clusters could be seen clearly. The border location was registered for each embryo as a vector between the center of the embryo and the edges of the cell cluster. The TE area covered by each clonal cell cluster was calculated as the angle formed between the vectors connecting the top of the cluster and the center, and the bottom of the cluster and the center. The clone forming each cell cluster (GFP+ and GFP-) was also annotated.

Clonal composition of the polar vs mural TE

Spot representations of the cells, as well as the actual Phalloidin signal (which reports cell borders), were used for the quantification of GFP+ and GFP- cells in the mural vs polar TE. The polar TE region was defined as the TE area containing cells that were in direct contact with the ICM. A surface reconstruction of each polar TE and ICM was prepared using the “Surface” tool on Imaris. These surfaces are included in Figure 2K. The number of GFP+ and GFP- cells in this area (polar TE) and outside of it (mural TE) were then calculated. We present data comparing the contribution of the ICM dominant population in the ICM and the contribution of the ICM dominant population in either the polar or the mural TE.

Cell cycle length

Movies of SiR-Actin and SPY555-DNA stained or unstained mouse embryos were used to assess the effect of dye staining on the division rate. The time at which each cell completed cytokinesis at the 4- to 8-cell division stage was recorded. Additionally, the time at which each cell completed cytokinesis at the 8- to 16-cell division was also recorded. Both values were used to measure the length of the 8- to 16-cell cycle, presented in the figures. The same process was performed to measure human cell cycle length at the 8- to 16-cell transition. Furthermore, individual cells from dyed embryos (both human and mouse) were observed to record the time at which the major phases of mitosis occurred (prophase, metaphase, anaphase, telophase and cytokinesis).

Lineage tree reconstructions from 1- to 16-cell stage using Embryoscope™ time-lapse movies

Embryoscope™ time-lapse movies capturing preimplantation development in human embryos from the zygote to blastocyst stage were provided by IVIRMA-Valencia (IVI Foundation, Spain). Each movie contained transmitted light images at 11 focal planes with an average imaging frequency of 15 minutes. All samples represented embryos that resulted in successful pregnancies and live births. Manual tree curation and division scoring was performed by two independent researchers, in two locations in a blinded manner using TrackMate.^{58,59} Division scoring was done before tree curation so that the assessors remained blinded to the clonal assignment of the assessed divisions. The following parameters were recorded: timing of division of each blastomere at 2-, 4- and 8-cell stage, clonal history of each cell, symmetric/asymmetric cell division history of each cell during 8- to 16-cell transition. It was not possible to trace cells and lineage fate beyond the 16-cell stage, due to the loss of single cell resolution on compaction. Fifty-four movies were of sufficient quality to annotate all required parameters with confidence and in agreement between the annotators.

Expected proportions in Figures 7D, 7E, and 7O were calculated using the probability mass function of the hypergeometric distribution (PMFHD):

$$P(x, M, K, N) = \frac{\binom{K}{x} \times \binom{M - K}{N - x}}{\binom{M}{n}}$$

where x is the number of ACDs (2 or 3) done by the same 2-cell clone, M is the number (8) of mother cells, K is the number (4) of same-clone mother cells and N is the number (2 or 3) of total ACDs per embryo.

PMFHD assumes that the outcome of one event modifies the probability of the subsequent events (e.g. If in one embryo with 2 ACDs the first cell that undergoes an ACD originates from the faster “A” 2-cell blastomere ($P = 4/8$ or 50%), the probability for the second ACD to be from the “B” clone is higher ($P = 4/7$ or 57.1%) than of that of it being from the “A” clone ($P = 3/7$, 42.9%)). For the expectation in Figure 7O, the fraction of total ($n = 46$) cases in which a distribution of embryos with 1, 2, 3 or 4 ACDs like the one measured in our sample (Figure 7C) would result in embryos with A>B, A=B or A<B inside cells was calculated. This is presented in the figure.

Detection of the presence of arrested blastomeres

Blastocyst images generated by us were used to detect the presence of large arrested blastomeres at the surface of the TE. For this, brightfield images were used, and large cell remnants that appeared arrested were quantified. Embryoscope™ time-course brightfield images of embryos developing from the zygote to the blastocyst stage were provided by IVIRMA-Valencia (IVI Foundation) (as described above) and were used to measure the number of embryos with arrested blastomeres. Movies were visually inspected using ImageJ and the presence of abnormally sized blastomeres with a darker or oddly textured appearance that arrested and did not divide further was recorded, as well as the number of embryo cells present at the time of the first appearance of such structures. Eighty-eight embryoscope movies were successfully analyzed for the presence of arrested blastomeres between the 2- and 16-cell stage.

Statistical model of blastocyst development with random cell arrest, death and internalization

We developed a Markov Chain Monte Carlo model of blastocyst development to study the distributions of GFP+ and GFP- cells in the whole embryo and in the ICM/TE in detail, ignoring geometrical or other spatial effects (with an exception detailed below). Using this model, we generated pools of 22 embryos. Each embryo starts at the two-cell stage, with one blastomere marked by GFP, and the other unmarked. The embryos then undergo consecutive rounds of cell division, during which the cell type (GFP+ or GFP-) is inherited by the daughter cells. At the 4-cell and 8-cell stages, we let a random subset of the blastomeres arrest (i.e., not divide any further), and from the 64-cell stage onward we let another random subset (possibly including already arrested cells) die. Both cell selection processes for arrest and death are assumed to be independent Bernoulli processes with probabilities p_{arrest} and p_{death} in each affected cleavage cycle. Thus, the fraction of blastomeres undergoing arrest or death is not fixed at p_{arrest} and p_{death} , but varies across these probabilities according to a binomial distribution. Cell arrest and death are assumed to occur to GFP+ and GFP- blastomeres, as well as to those in the ICM and TE, with equal chance.

In the absence of detailed information regarding non-uniformity in cell death over space and time, other than that it is observed primarily after the morula stage, we assume cell death to occur only from the 64-cell stage onward at a constant rate p_{death} . We set $p_{\text{death}} = 4.4\%$, such that the average percentage of dead cells at the blastocyst stage lies in the middle of the previously reported range of 7-8%⁴² (Figure 6A). Meanwhile, the selected rate of cell arrest $p_{\text{arrest}} = 6.5\%$ is based on a maximization of the statistical agreement between the model prediction and the data (Fig. Figure 6B), as quantified by the harmonic mean P -value from four two-sample Kolmogorov-Smirnov tests that compare the clonal distributions across the whole embryos, the distributions of relative ICM sizes, and the distributions of the shares of the ICM dominant clone in the TE and ICM (Figures 6C–6E):

$$P^\circ = \frac{4}{\sum_{i=1}^4 1/P_i}.$$

The identified optimum of 6.5% that maximizes P° lies well in the range of the previously reported rates of 4.3% and 8.3% for the 4- and 8-cell stages.⁴³

After the 3rd, 4th and 5th round of cell division (*i.e.*, during the 8- to 16-, 16- to 32- and 32- to 64-cell stage transitions), we randomly select a subset of the daughter blastomeres and internalize them, generating a potential lineage imbalance. From this stage onward, the ICM and TE cell pools continue dividing separately. The number of cells internalizing, n_{inter} , like the arrest and death rates, is not fixed, but drawn uniformly within a predefined range [n_{\min}, n_{\max}] in each cleavage generation. Based on our observations in human embryos, we set n_{\min} to 1,0,0 and n_{\max} to 3,2,1 in the three cleavage rounds with cell internalization, and zero before and after. This approximately reproduces the observed final fraction of ICM cells as 17.4% of the total cells on average (Figure 6D). Only blastomeres with distinct mother cells are eligible for internalization, to mimic asymmetric division in which just one out of the two sister cells internalizes per cycle. A fourth model parameter, the fate determination bias b , controls the average ratio between internalization of GFP+ and GFP- cells. For unbiased selection (equal average likelihood for GFP+ and GFP- blastomeres to internalize), $b = 0.5$, whereas $b = 1$ represents exclusive internalization of one of the two cell types. The biased average internalization numbers are thus given by bn_{inter} and $(1 - b)n_{\text{inter}}$ for the respective cell types.

Motivated by a potential buffering role of geometric constraints on the number of internalizing blastomeres, our model additionally includes a “memory effect” to partially compensate in subsequent cycles for relatively few or many asymmetric cell divisions in previous cycles. The deviation in the cumulative expected mean number of internalized blastomeres from the actually realized cumulative sum until generation i ,

$$\sum_{j=3}^i \frac{n_{\min,j} + n_{\max,j}}{2} - n_{\text{inter},j},$$

is added to the next number of internalizing cells, $n_{\text{inter},i+1}$. Since cell numbers approximately double in each generation, the impact of this compensation on the size of the ICM halves in each generation.

Once each embryo reaches the final number of blastomeres as observed in the human dataset, we sort them by their contribution of GFP+ cells. Repeating this stochastic process 10⁴ times allows us to evaluate the statistically expected distribution of GFP+ and GFP- cells in the whole embryos, and in the ICM and TE individually.

We recorded the clonal composition at early stages, for example after the first internalization wave at the 16-cell stage. We then compared the clonal composition at early stages to the final outcome at the blastocyst stage, to study the importance of early ACDs. We observed that an existing clonal imbalance at the 16-cell stage is a strong predictor of the clonal dominance in the ICM at the blastocyst stage in both the unbiased and biased models (Figure 7G). In 87.5% of all 220,000 simulated embryos without fate bias (89.9% for the model with 70% bias), the embryos with a clonal imbalance at the 16-cell stage developed into blastocysts with the same clone dominating the ICM.

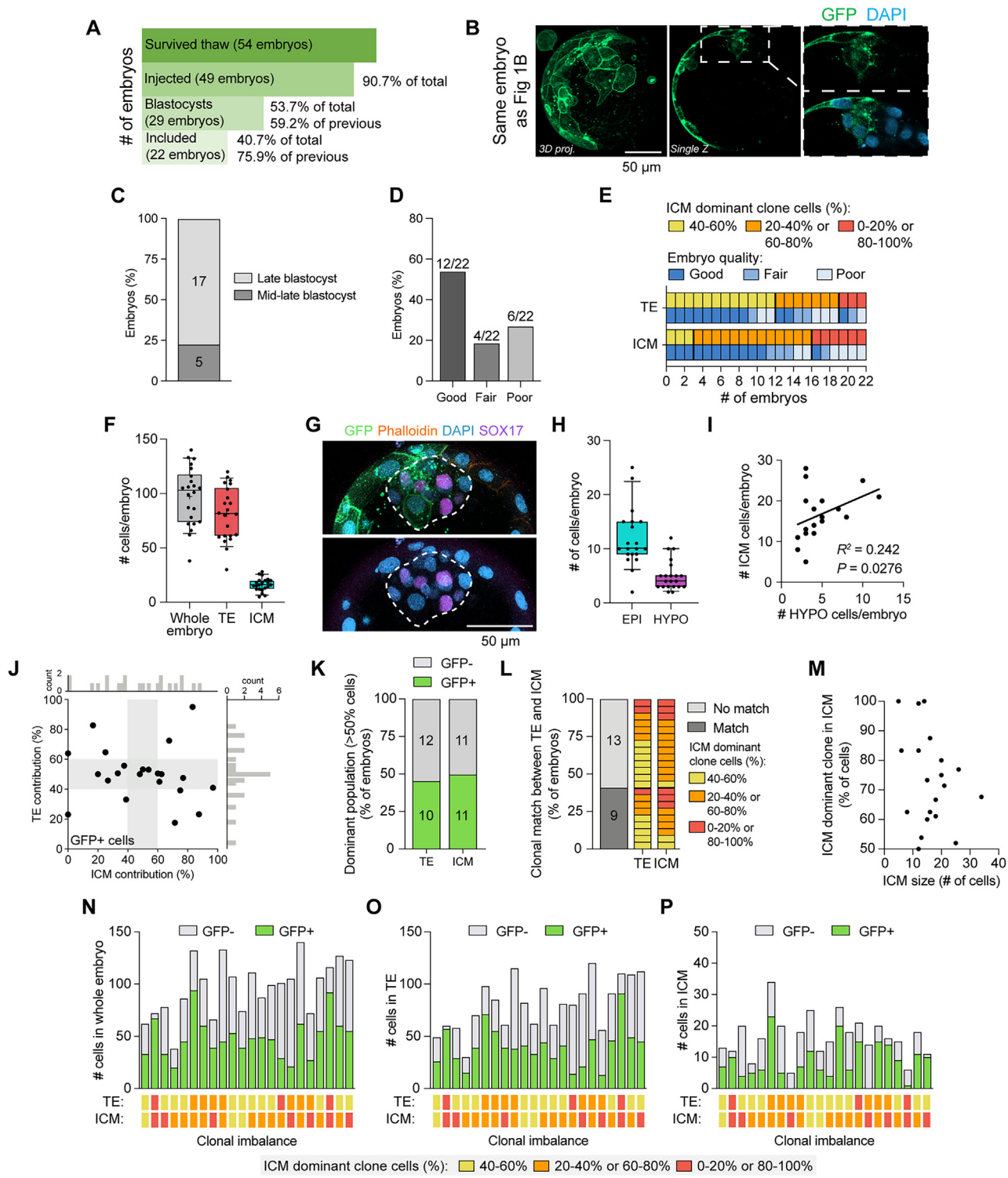
To verify whether there are any statistically significant differences in the two human embryo datasets that were used in this study, we used a subset of the simulated embryos that had the exact clonal compositions at the 16-cell stage as those observed in the Embryoscope™ movies, and compared the blastocysts they develop into according to the biased and unbiased models to the blastocysts observed in the labelled dataset (Figure 7C). No statistically significant differences were found in the compositions of the TE or ICM of the resulting blastocysts.

Finally, we validated our model against a published dataset that tracked mouse blastomeres in embryos from the 2 to 32-cell stages.¹⁵ The model that best recapitulates the published data is one with no fate bias ($b = 0.5$), $n_{\text{inter}} = 1$ in the 1st internalization wave (8 to 16 cells), and $n_{\text{inter}} = 8 - 12$ in the 2nd wave (16 to 32 cells). The corresponding P -values analogous to Figure 6 are $P_1 = 0.46$, $P_2 = 0.63$, $P_3 = 0.63$, $P_4 = 0.10$, suggesting that our model for human embryo development is also capable of reproducing early mouse embryogenesis within the range of statistical errors and with appropriately adjusted numbers of ACDs (Figure S8).

P -values of statistical comparisons were either directly evaluated from the results of the 10⁴ model realizations (as the probability of the model predicting values at least as extreme as observed in the data), or calculated with two-tailed Kolmogorov-Smirnov tests, as indicated in the figure captions.

Custom MATLAB code can be found in the supplementary materials, or at: https://git.bsse.ethz.ch/iber/Publications/2024_junyent_meglicki_blastomeres

Supplemental figures



(legend on next page)

Figure S1. Details on the quantification of the clonal imbalances of human blastocysts, related to Figure 1

- (A) Breakdown of the embryos used for this project, including the number of embryos that survived thawing, that were microinjected, that developed to blastocysts, and that were included in the final quantification. Rules for inclusion/exclusion are listed in the [STAR Methods](#).
- (B) Representative example of a human blastocyst with mosaic expression of GFP (same embryo as shown in [Figure 1B](#)) with only DAPI staining (blue) and GFP (green) shown. Scale bars, 50 μ m.
- (C–E) Qualification of the blastocysts included in the analysis following the Gardner and Schoolcraft blastocyst grading system. (C) Percentage of embryos that were mid-late or late blastocysts at the time of fixation. (D and E) Percentage and number of embryos that were qualified as in “good,” “fair” or “poor” fitness at the blastocyst stage (details in the [STAR Methods](#)). $n = 22$ human embryos. In (E) embryos are colored according to their degree of clonal imbalance.
- (F) Quantification of the number of total cells (gray), trophectoderm cells (red), and inner cell mass cells (ICM, blue) in the blastocyst images. Error bars are 10–90 percentile, box is upper and lower quartiles, and center line is median. $n = 22$ human embryos.
- (G) Representative maximum intensity projection (MIP), showing the expression of SOX17 in a subset of cells of the ICM (indicated by white dashed line). Embryos expressed mosaic GFP and were stained for AF647-phalloidin (orange) and DAPI (blue). Scale bars, 50 μ m.
- (H) Quantification of the number of epiblast cells (cyan) and hypoblast cells (purple) in the blastocyst images. Error bars are 10–90 percentile, box is upper and lower quartiles, and center line is median. $n = 20$ human embryos. For (H) and (I), two embryos from test experiment were not included in the analysis because they were not accessible for SOX17 staining.
- (I) Scatterplot indicating the correlation between the number of hypoblast cells per embryo versus the number of cells in the ICM for that embryo. Trend line indicates linear regression. R^2 and p value against a line with zero slope are displayed in the figure. $n = 20$ human embryos.
- (J) Scatterplot presenting the percentage of GFP+ cells in the TE and ICM of each of the embryos analyzed. $n = 22$. Gray bands indicate 40%–60% windows (low clonal imbalance). Marginal histograms report the counts.
- (K) Plot presenting the percentage of embryos for which GFP+ (green) cells or GFP– (gray) cells are dominant in the whole embryo. The dominant population is defined as the population that contributes >50% of cells in the embryo. $n = 22$ human blastocysts.
- (L) Plot presenting the percentage of embryos that have matching (dark gray) or non-matching (light gray) populations in the TE and ICM. In matching embryos, the same 2-cell clone is the dominant (>50% of cells) population in the ICM and the TE. Side bar indicates, with colors, the degree of clonal imbalance of each individual embryo contained in the previous quantification. $n = 22$ human blastocysts.
- (M) Scatterplot displaying the ICM size counted in absolute number of cells in relation to ICM dominant clone contribution to the ICM. $n = 22$ human blastocysts.
- (N–P) Bar plots depicting the number of GFP+ and GFP– cells in the whole embryo (N), the TE (O), and the ICM (P) for each embryo analyzed. Boxes underneath indicate the degree of clonal imbalance in the ICM or TE of each embryo. $n = 22$ human blastocysts.
- For all applicable panels, numbers in columns indicate the embryo number.

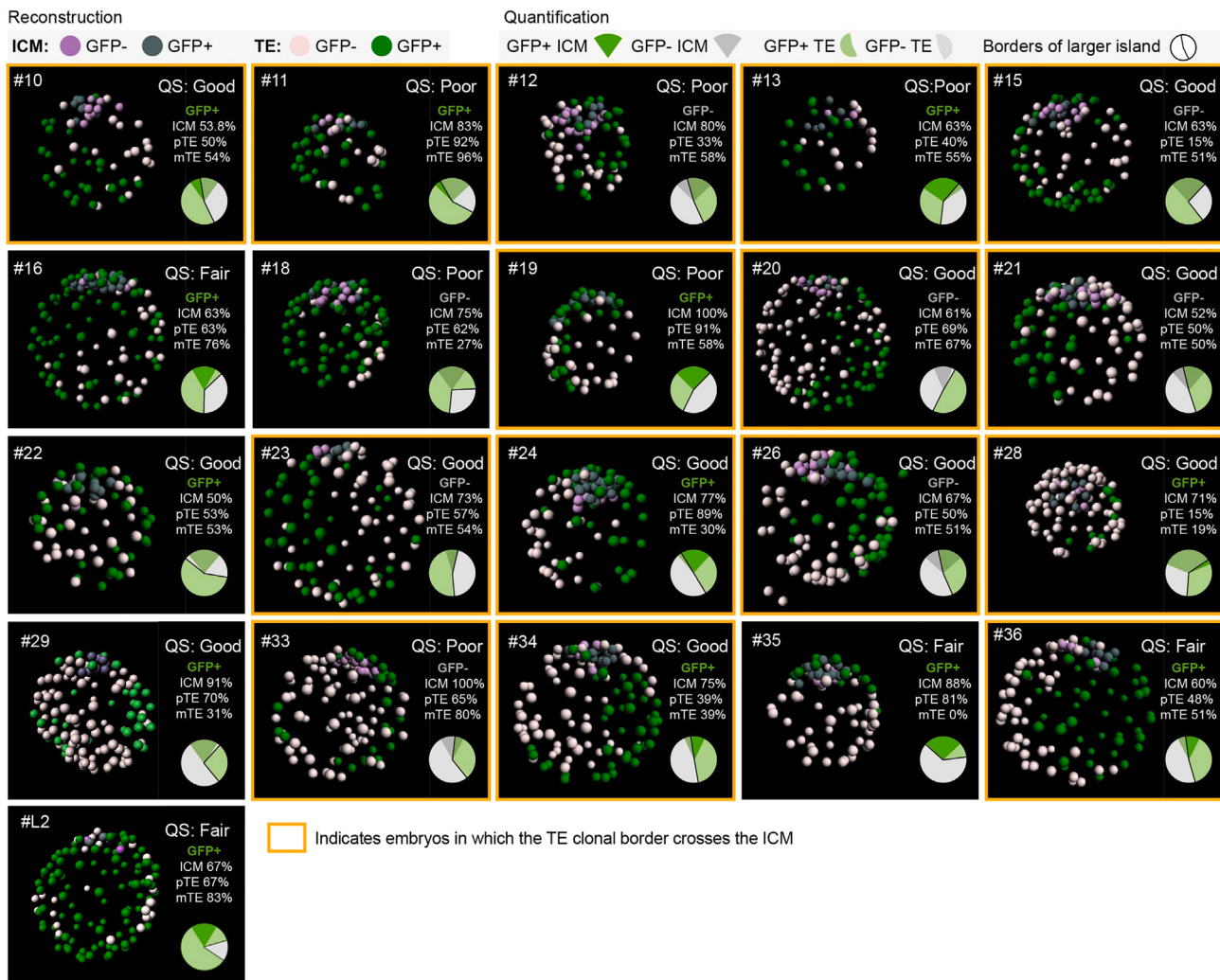
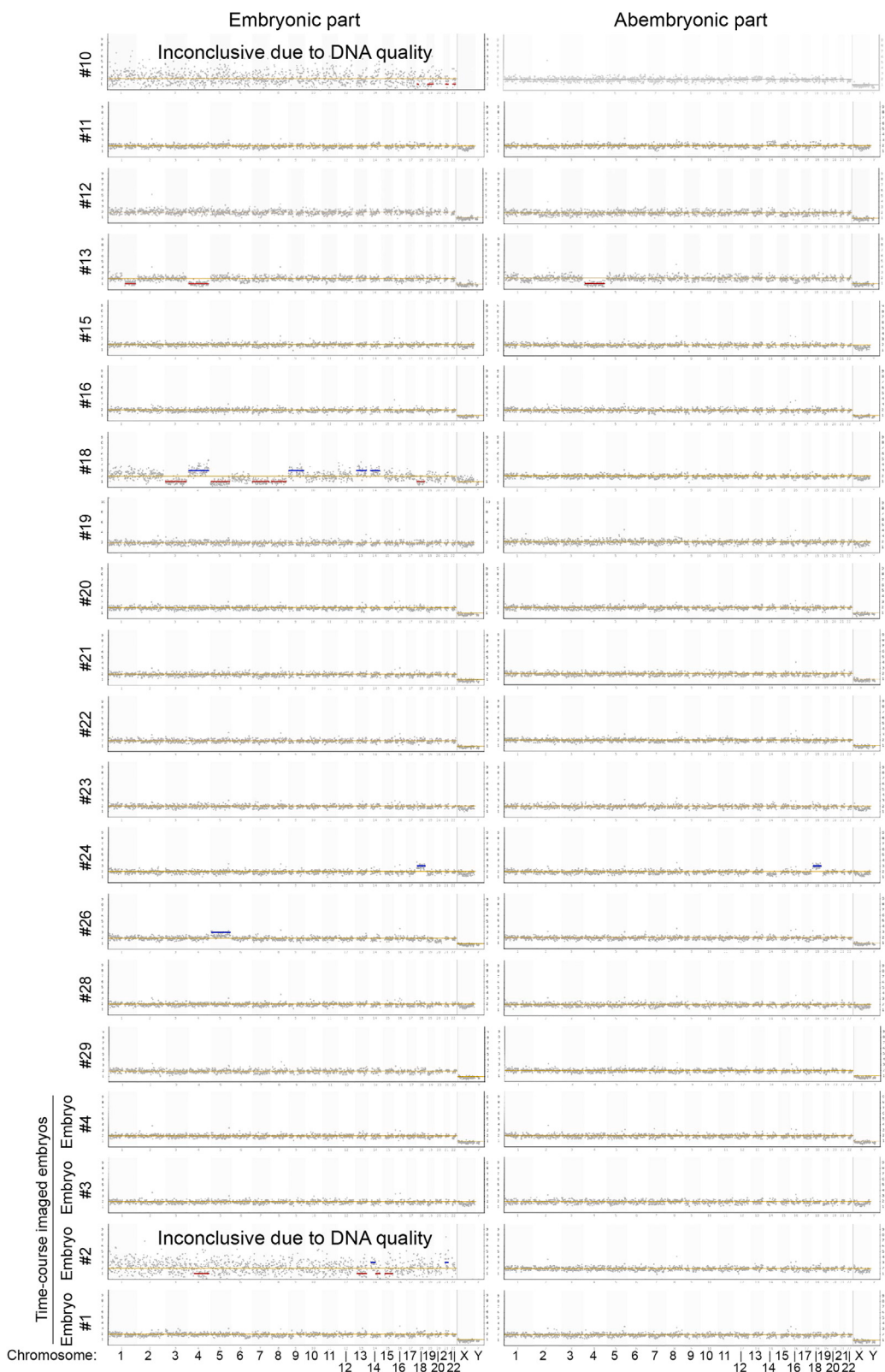


Figure S2. Reconstructions of the human blastocysts analyzed, related to Figure 2

Reconstructions of the position of GFP+ and GFP- cells in the human blastocysts. Spots indicate cell centers and are colored according to GFP expression and position (ICM or TE), as indicated in the legend. Insets show the quality score (QS) classification, percentage of either GFP+ or GFP- cells in the ICM, polar TE (pTE) or mural TE (mTE), and a circular plot depicting the area occupied by the ICM and the TE area covered by the largest GFP+ and GFP- cell cluster. Yellow frame indicates embryos in which the TE clonal border crosses the ICM. One embryo was excluded as it was damaged during sample processing, which precluded us to perform this analysis.



(legend on next page)

Figure S3. Karyotyping human blastocysts, related to Figure 3

Plots presenting the DNA sequencing results for the embryos presented in [Figure 3J](#). For two embryos (#2 and #10), the embryonic part sequencing results were designated as unreliable by a technical expert. For all plots, orange line set at 2 indicates euploidy (n_2 diploid chromosome count), monosomies (n_1) are indicated with a red line, and trisomies (n_3) are indicated with a blue line. Chromosomes are labeled in the x axis. Two embryos could not be included in the analysis.

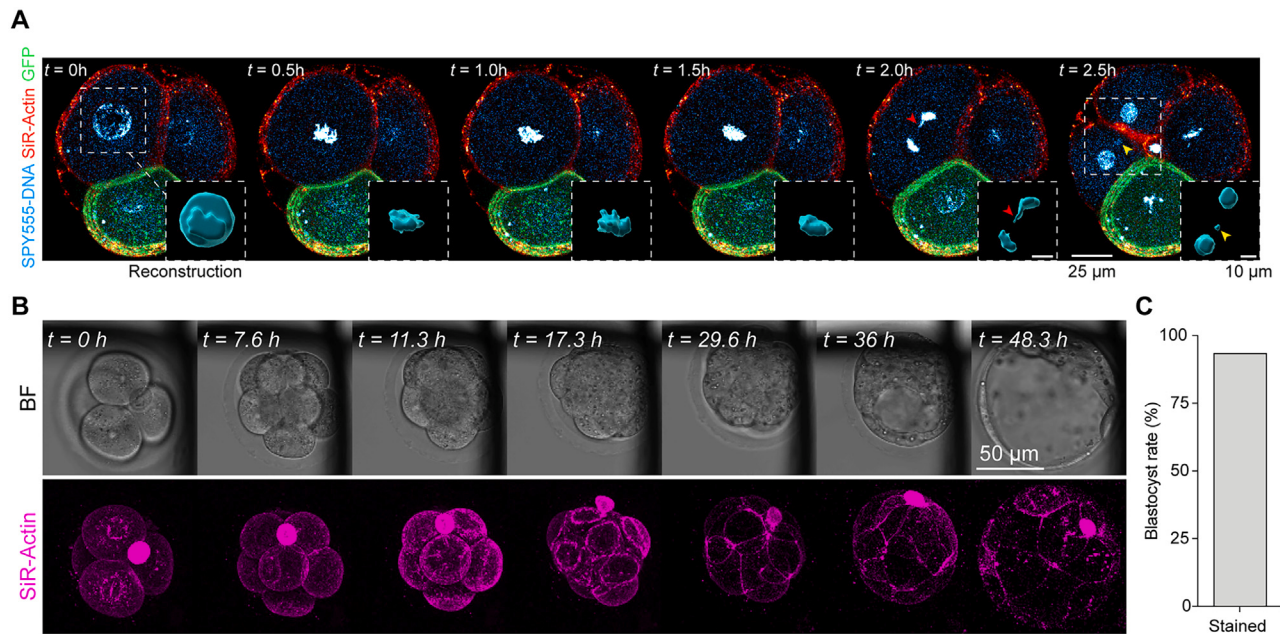


Figure S4. Staining of human and mouse embryos with SiR-actin and SPY555-DNA, related to Figure 4

(A) Representative frames of a time course imaging of an example of a human embryo with lagging chromosome at the 4-cell stage. Embryos mosaic for GFP was stained with SiR-actin and SPY555-DNA and imaged. Dashed white box is the reconstruction of the SPY555-DNA signal, indicating a lagging chromosome (red arrowhead) and the presence of a cytoplasmic DNA (cytDNA). This embryo arrested and degenerated before reaching blastocyst stage and thus was not included in the final analysis. Zona pellucida was digitally removed during image processing. Scale bars, 10 or 25 μm , as stated in the figure.

(B) Representative frames depicting a mouse embryo stained with SiR-actin and developing until the blastocyst stage. Scale bars, 50 μm .

(C) Percentage of mouse embryos stained with SiR-actin that develop to the blastocyst. $N = 17$ embryos imaged from the 2-cell stage.

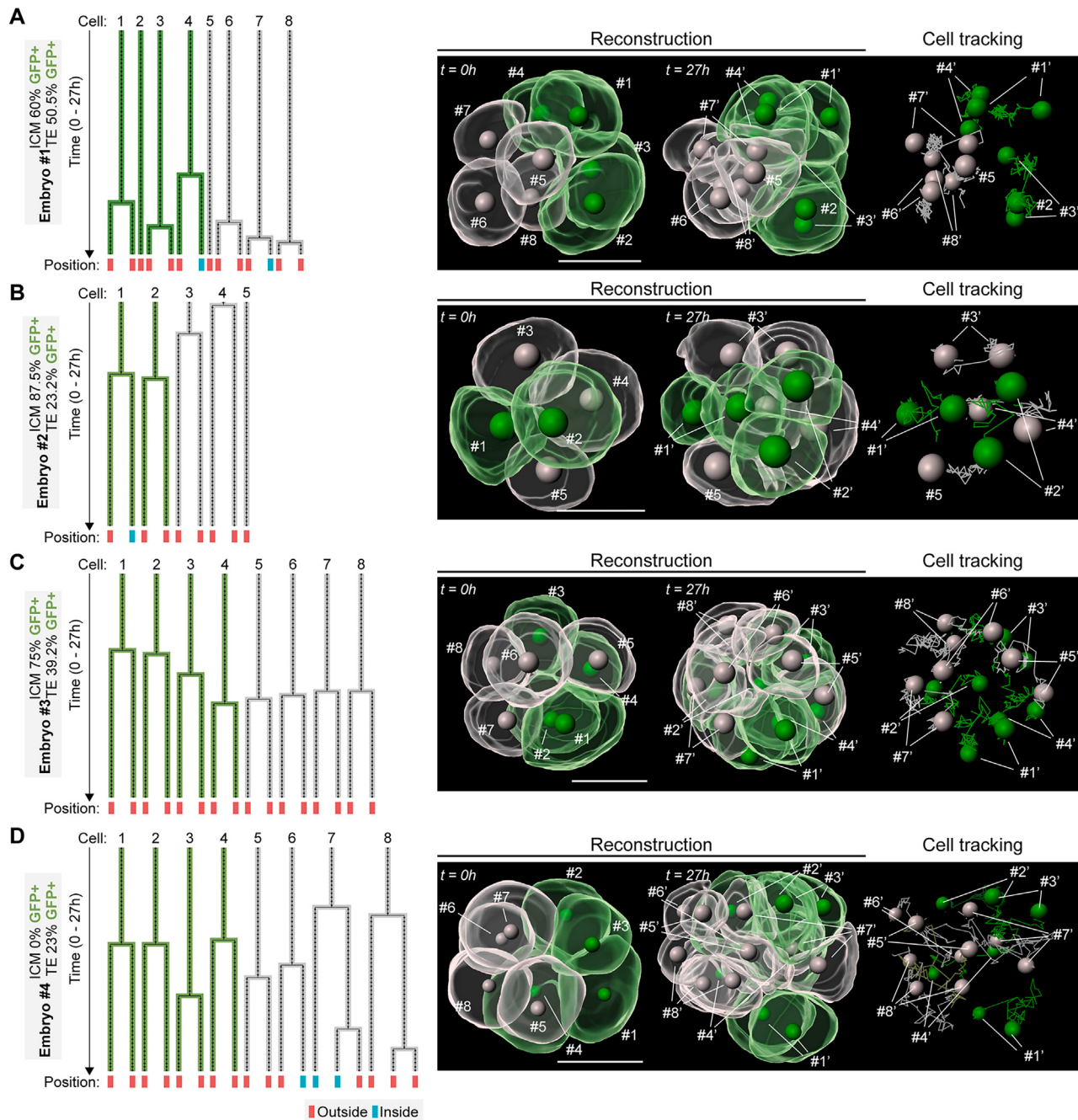


Figure S5. Lineage tracing of 8- to 16-cell transitions in human embryos, related to Figure 5

(A-D) Details corresponding to the cell tracking on the four embryos shown in Figure 5. (Left) Trees generated by lineage tracking: Branches indicate divisions, spots indicate time points, and bottom squares indicate the final position of the cell (outside: red, inside: blue). Gray squares on the side indicate final ICM and TE composition quantified at the blastocyst stage for those embryos. (Right) Reconstructions of the embryos analyzed for the first ($t = 0\text{ h}$) and last ($t = 27\text{ h}$) time point. GFP+ cells are reconstructed in green, and GFP- are gray. Annotations in the images refer to the lineage trees. Numbers with an apostrophe indicate daughter cells from the same division. The last panel displays the ball and chain representation of the cell movement over time. (D) is also shown in Figure 5. Scale bars, 50 μm .

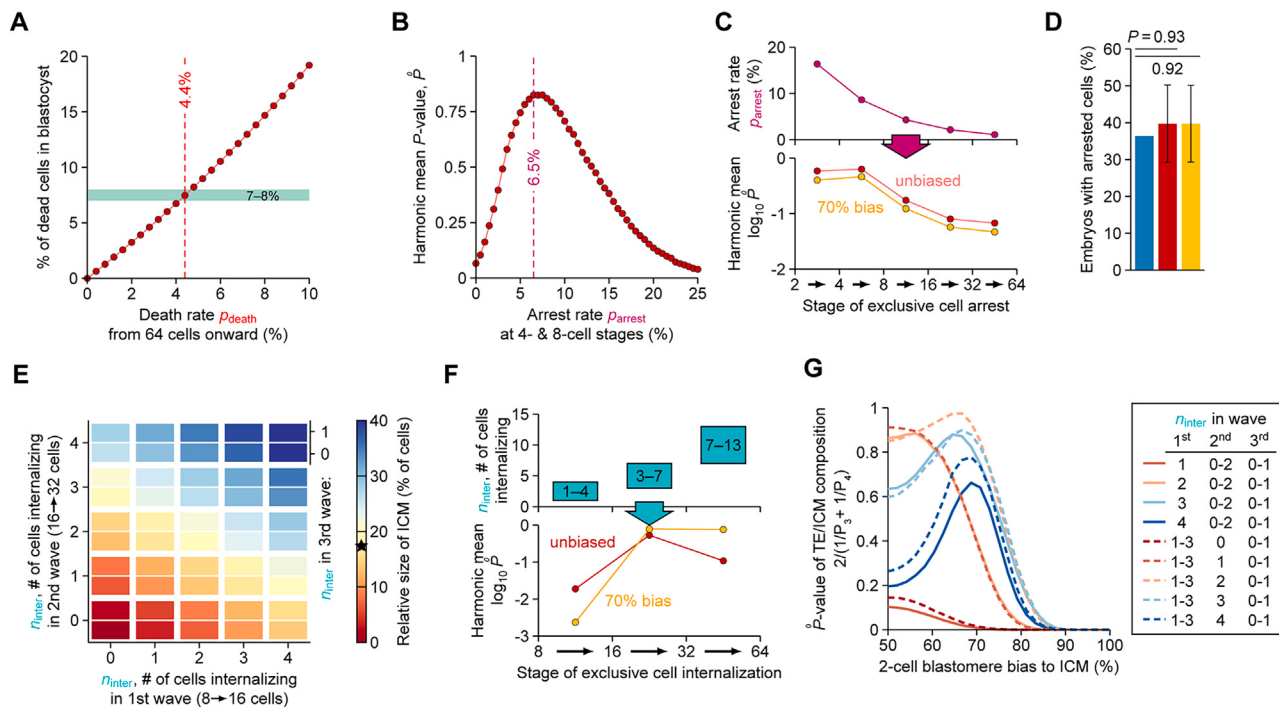


Figure S6. Additional modeling parameters, related to Figure 6

(A) Percentage of dead cells in the blastocyst as a function of the death rate (p_{death}) applied from the 64-cell stage onward. A p_{death} of 4.4% results in 7%–8% dead cells in the blastocyst, as in Brison.⁴²

(B) Dependency of the statistical consistency on the cell arrest rate applied at the 4- and 8-cell stage. Harmonic mean \bar{P} (as defined in Figure 6) is maximal at an arrest rate of 6.5%.

(C) Dependency of blastocyst development on the time point of cell arrest. Arresting cells exclusively at single-cell stages with the probability p_{arrest} (top) required for the correct percentage of embryos with arrested blastomere(s), as in (D), leads to mild reduction in overall statistical agreement between model and data (bottom). Early arrest is statistically favored. In the bottom, colors indicate results using the unbiased (red) or 70% biased (yellow) model.

(D) Proportion of actual (blue) or modeled embryos with at least one arrested blastomere in an unbiased (red) or 70% biased (yellow) model. The arrest rate calculated in (B) was applied at the 4- or 8-cell stages. Bars are mean, error bars are SD. Two-sided p value evaluated directly as the probability of observing a value at least as extreme in the 220,000 modeled embryos.

(E) Heat plot indicating the modeled size of the ICM using the unbiased model when the number of internalized cells (n_{inter}) in the first (8- to 16-cell), second (16- to 32-cell), or third (32- to 64-cell) wave of ACD is modulated. Box color indicates ICM size as the percentage of blastocyst cells. Black star indicates the size calculated from the labeled embryos (17.4%).

(F) Robustness of blastocyst development to changes in the time point of cell internalization. Internalizing cells exclusively at single-cell stages in numbers n_{inter} (top) required for the correct ICM size as in Figure 1D, largely preserves the overall statistical agreement between model and data (bottom) only in the unbiased case. Later internalization requires stronger fate bias to explain the observed data. Forced early internalization makes a bias less likely.

(G) Statistical (dis)agreement between observed and modeled embryos under perturbation of the internalization numbers n_{inter} and modeled fate bias. When many cells internalize in the same wave (blue), the observed clonal composition in the TE and ICM is best reproduced by a model with 65%–70% fate bias, as otherwise the ICM composition is too balanced. Internalizations spread more uniformly across waves (red) make a fate bias less likely. Very few ACD in the first two waves are generally unlikely.

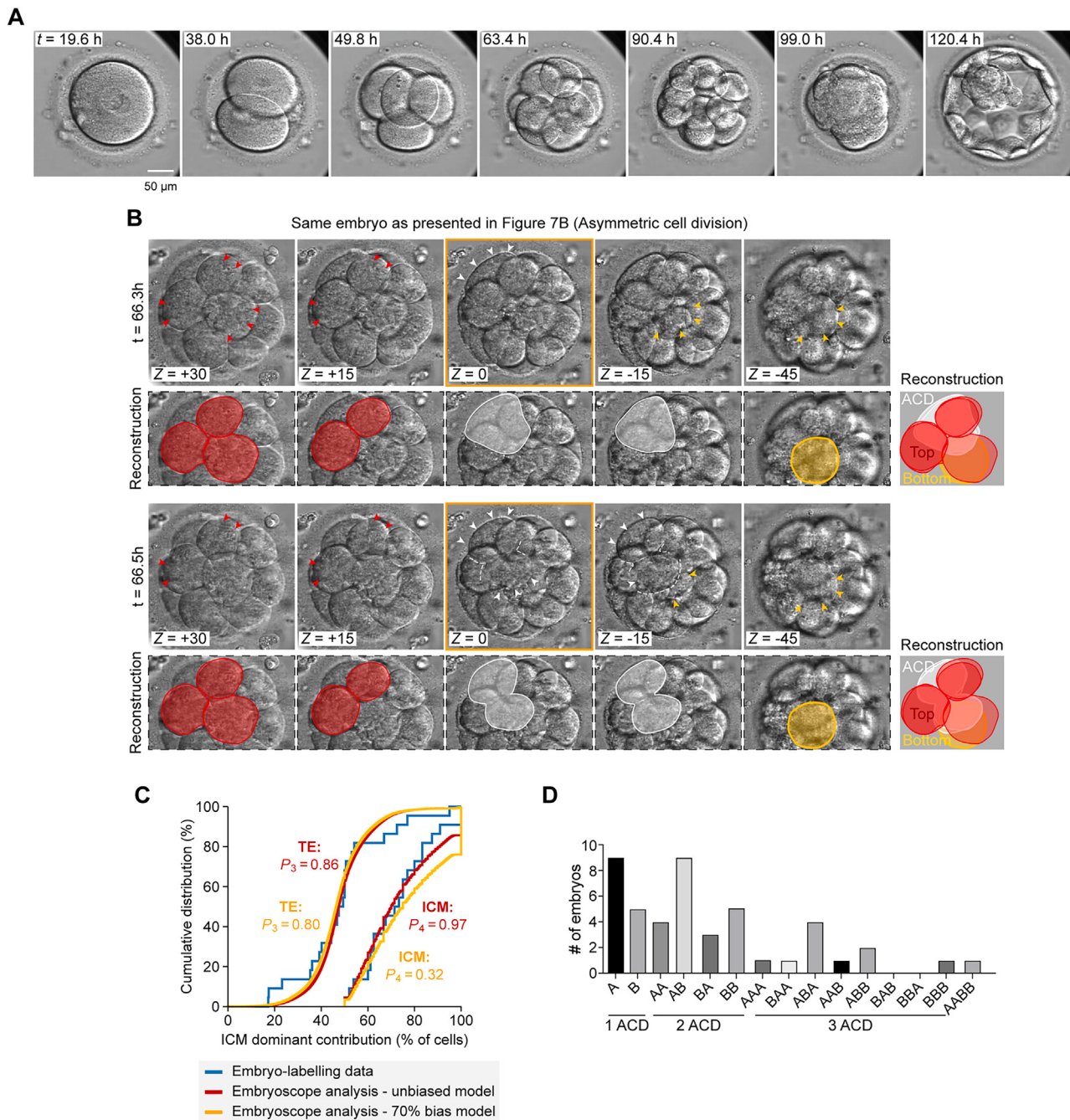


Figure S7. Embryoscope lineage tracing, related to Figure 7

(A) Representative frames from multifocal Embryoscope transmitted light time-lapse movies used in the study, covering preimplantation development of human embryos from zygote to blastocyst stage. Representative single focal planes and time points were selected for the purpose of this example. t, absolute time included in the embryoscope movie.

(B) Representative example of an asymmetric (inside-outside) cell division analysis presented on main Figure 7B, tracked in multifocal Embryoscope transmitted light time-lapse movie. Five different focal planes (Z) are presented. Top panel shows time point ($t = 66.3\text{ h}$) before asymmetric cell division and bottom panel shows a time point (66.5 h) after one of the blastomeres has divided asymmetrically. Cell dividing asymmetrically is segmented in gray, cells at the bottom and top of the embryo are segmented yellow and red, respectively. Segmented cells are reconstructed on the right. t, absolute time provided with the embryoscope movie. Yellow box highlights the plane presented in Figure 7B.

(C) Developing the embryos with their exact clonal compositions from the Embryoscope dataset from the 16-cell stage to the blastocyst stage with the statistical model results in distributions in the TE and ICM (red and yellow) that are statistically compatible with those observed in the labeled embryos (blue, as in Figure 6E).

(D) Quantification of the percentage of human embryos with different number of ACDs (asymmetric cell divisions) during 8- to 16-cell division and with different patterns and order of faster (A) and slower (B) 2-cell clone contribution to ACDs. Blastomere identity (A) was assigned as given in Figure 7I. $n = 46$ human embryos.

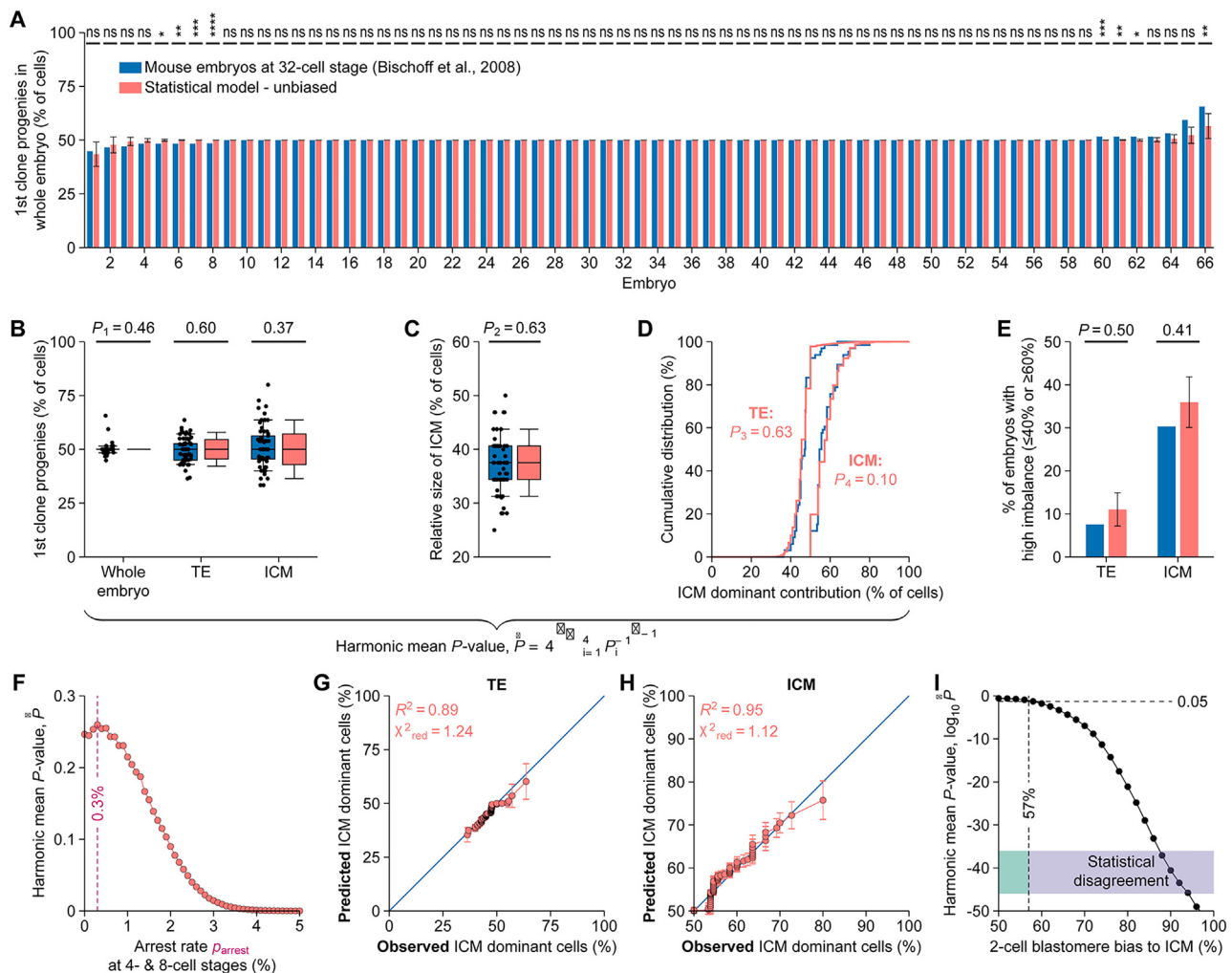


Figure S8. Validation of the model against a dataset of 32-cell stage mouse embryo composition related to STAR Methods

(A) Comparison of observed (blue) and statistically predicted (unbiased, pink) distributions of “1st clone” progenies in 66 whole blastocysts, showing few statistically significant deviations. Observed data was extracted from Bischoff et al.,¹⁵ and 1st clone was the nomenclature used in the original publication to label 1 2-cell blastomere. Model predictions in (A) and (E) are mean \pm SD from 10^4 statistically independent realizations of the 68 blastocysts. All p values in (B) (evaluated directly from the fraction of 10^4 model predictions equally or more extreme than the observation) are $p > 0.05$ (ns), $p < 0.05$ (*), $p < 0.01$ (**), $p < 0.001$ (***)�.

(B) Distributions of 1st clone contributions by tissue, showing no statistically significant deviations between actual data and model. In (B) and (C), error bars are 10–90 percentile, box is upper and lower quartiles, and center line is median. All p values in (B)–(D) are from two-sample Kolmogorov-Smirnov tests.

(C) Relative size of the ICM, showing no statistically significant deviations between data and model.

(D) 1st clone contributions in the TE and ICM, showing no statistically significant deviations between data and model.

(E) Percentages of embryos with a 1st clone contribution $\geq 60\%$ in the ICM, or $\geq 60\%$ or $\leq 40\%$ in the TE, which indicates clonal imbalances. Figure shows no statistically significant deviations between data and model.

(F) Dependency of the statistical consistency on the cell arrest rate applied at the 4- and 8-cell stage. Harmonic mean P^* is maximal at an arrest rate of 0.3%. (G and H) P-P plots showing the predicted fraction of 1st clone cells in the TE and ICM against the observed fraction. Each data point represents one of the 66 blastocysts with statistical mean values μ_i and SDs σ_i as error bars. The data do not deviate significantly from a diagonal line. R^2 is the coefficient of determination.

$\chi^2_{\text{red}} = \frac{1}{66} \sum_{i=1}^{66} \left(\frac{x_i - \mu_i}{\sigma_i} \right)^2$ is the reduced chi-squared test statistic, which is low in absence of statistical disagreement.

(I) Overall degree of statistical consistency between data and model, measured by the harmonic mean of four p values from (B) (whole embryo), (C) (ICM size), and (D) (TE and ICM clonal distribution), as a function of the 2-cell clonal fate bias to become ICM. At about a 57:43 bias, the $P^* = 0.05$ threshold is crossed. Therefore, an unbiased model was used throughout the figure. Overall, our model for human embryo development is also capable of reproducing early mouse embryogenesis within statistical errors and with appropriately adjusted numbers of ACD.